Thermal Science and Engineering Progress 55 (2024) 102967

Contents lists available at ScienceDirect

Thermal Science and Engineering Progress

journal homepage: www.sciencedirect.com/journal/thermal-science-and-engineering-progress

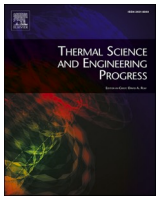

Strength analysis due to thermal loading and tensile loading when metals are bonded by heat-curing adhesives

Kazuhiro Oda [a,*], Hiroki Oda [a], Yasushi Takase [b], Nao-Aki Noda [b,*]

[a] Division of Mechanical Engineering, Faculty of Science and Technology, Oita University 700 Dannoharu, Oita 870-1192, Japan
[b] Department of Mechanical Engineering, Kyushu Institute of Technology, 1-1 Sensui-cho, Tobata-ku, Kitakyushu-shi, Fukuoka 804-8550, Japan

ARTICLE INFO

Keywords:
Heat-curing adhesives
Strength analysis
Thermal stress
Butt joint
Thermal and mechanical loadings
Thermal stress intensity factor

ABSTRACT

Heat-curing adhesives are widely used after being cured by heating to a temperature higher than room temperature. To evaluate the adhesive strength, therefore, it is necessary to consider both the thermal stress generated during heat curing and external loads such as tensile stress. Butt joint specimens are essential for evaluating tensile adhesive strength but also thermal strength. The interfacial strength can be discussed from the stress intensity factor (SIF) of a fictitious edge interfacial crack assumed at the interface end. This is because the SIF is controlled by the intensity of singular stress field (ISSF) at the crack-free interface end and a constant term associated with the thermal load. In this paper, a useful thermal SIF solution is proposed by superposing the SIF under tensile stress and the SIF under uniform interface stress associated with thermal loading. This general SIF expression provided under arbitrary material combination can be applied for predicting the tensile strength σ_c and critical temperature change ΔT without performing new FEM calculations. The usefulness of the expression is confirmed through the adhesive strength of Aluminum/Epoxy butt joint experimentally obtained. Once the critical SIF K_{1C} can be obtained from the tensile strength σ_c and the temperature change ΔT, the adhesive strength can be expressed as K_{1C} = constant of an assumed fictitious interface, and this can be used to predict critical σ_c for various temperature change ΔT and for various adhesive bondline thickness h.

1. Introduction

Adhesive joints offer lots of advantages such as improved appearance, excellent sealing properties, high strength/weight ratio, and relatively low stress concentration. For this reason, in recent years, the use of adhesives for assembly structural members has become widespread in various industrial fields. For example, in recent years, they are primarily used in aircraft and vehicle construction to join metallic and non-metallic parts and to attach microchips to printed circuit boards [1–6]. To evaluate adhesive strength, the fictitious crack modeling as shown in Fig. 1 has some advantages. For example, (1) The original singular stress field without crack is not necessarily to be analyzed. (2) Although several problems whose original singular stress fields without crack are different, fictitious cracks always provide the same singular fields, which are controlled by the SIFs. (3) If the critical SIF is obtained from the maximum load for one problem, the critical SIF = const can be applied to other problems since they have the same singular fields.

It should be noted that the edge crack under thermal load in Fig. 1(a) and the edge crack under tensile load in Fig. 1(b) have some similarity but also have some difference. Thermal stress causes failure in dissimilar materials and electronic devices because of the elastic-thermal mismatch of the joined materials induces singular stress field at the edge of the interface [7–12]. Munz et al. [13–19] presented asymptotic solutions of thermal singular stress fields generated at joint corners for AB joint due to uniform temperature change stating that specific constant terms are included in thermal stress. Chen et al. [20,21] analyzed two-layer and three-layer adhesive plates, which are corresponding to AB joint and ABA joint, subjected to uniform temperature change clarifying the intensity of the singular stress field (ISSF) for arbitrary material combinations. Qian-Akisanya [22,23] and Reedy [24] analyzed the ISSF, which is named H parameter to estimate the adhesive joint strength under thermal stress.

In the authors previous study [25], the difference of the stress intensity factor (SIF) was discussed in the AB joint. Fig. 2 shows F_1, F_2 of the edge interface cracks in the AB joint. Note that the AB joint is equal to the ABA joint when $h/W \geq 1$ in Fig. 1. As shown in Fig. 2, regarding the singular stress fields of the AB joint, the followings are known [25].

* Corresponding authors.
E-mail addresses: oda-kazuhiro@oita-u.ac.jp (K. Oda), nao592noda@gmail.com (N.-A. Noda).

https://doi.org/10.1016/j.tsep.2024.102967
Received 21 February 2024; Received in revised form 24 September 2024; Accepted 5 October 2024
Available online 9 October 2024

Nomenclature

a	Length of the interface edge crack in the unknown problem
$2a^*$	Length of the interface crack in the reference problem
C_1, C_2	Dimensionless factors for short interface edge crack based on a/W
C_1^*, C_2^*	Dimensionless factors for short interface edge crack based on a/h
E	Young's modulus
e	Minimum element size at the crack tip in the unknown problem
e^*	Minimum element size at the crack tip in the reference problem
F_1, F_2	Dimensionless SIFs for interface crack based on applied stress
F_σ	Dimensionless ISSF at the interface end based on W
F_σ^*	Dimensionless ISSF at the interface end based on h
G	Shear modulus
h	Bondline thickness of butt joint
K_1, K_2	SIFs of an interface crack in the unknown problem
K_1^*, K_2^*	SIFs of an interface crack in the reference problem
K_σ	ISSF at the interface end
r	Distance from the interface crack tip
T_0	Temperature
T, S	Tensile and shear stresses applied to the reference problem
W	Width of the bonded plate
α, β	Dundurs composite parameter
ΔT	Uniform temperature change
ε	Oscillation singular index of an interface crack
η	Thermal expansion coefficient
σ	Applied remote stress
σ_{y0}	Equivalent stress associated with thermal loading
$\sigma_y(r)$	Singular stress along the interface
$\sigma_{y0,FEM}$, $\tau_{xy0,FEM}$	Stress values at the crack tip node calculated by FEM in the unknown problem
$\sigma^*_{y0,FEM}$, $\tau^*_{xy0,FEM}$	Stress values at the crack tip node calculated by FEM in the reference problem
λ	Order of the stress singularity at the interface end without the crack
ν	Poisson's ratio

Abbreviations

AB joint	Bi-material joint made of materials A and B
ABA joint	Butt joint using adherend A and adhesive B
SIF	Stress intensity factor
ISSF	Intensity of singular stress field

1) Under the same value of Dundurs parameter, the singularity exponents at the interface end are the same.
2) Under the remote tensile stress named equivalent stress σ_{y0}, the ISSFs are the same when no crack.
3) Even under the same ISSFs, the singular stress distributions in Fig. 1 (a) and Fig. 1(b) are totally different. This is because under the thermal loading, a large tensile stress often appears only near the surface, but a compressive stress appears inside [25].

However, to design real adhesive structures, butt joints (named ABA joints in this study) are essential. This is because the tensile adhesive strength σ_c obtained for ABA joint has been used. Similarly, to evaluate the adhesive strength under thermal loading, it is necessary to understand the specific thermal singular stress field of ABA joints. For example, it was reported that the ISSF varies depending on the adhesive layer thickness in the ABA joint under tensile load [26,27]; however, there is no systematical study of the SIF by varying the crack length, the adhesive layer thickness under arbitrary material combination.

Therefore, in this study, interface edge cracks in the ABA joints subjected to thermal stress will be analyzed. The thermal stress problem can be represented by superposing the tensile load problem the uniform stress problem. For this purpose, consider the ABA joints under tensile loads first. Then, the effects of crack length and adhesive layer thickness on the SIF will be investigated. Next, consider the ABA joints under thermal stress under arbitrary material combination. Finally, the validity of the SIF obtained will be confirmed through the experimental results [23] by assuming a fictitious crack. The discussion in this paper is especially useful for heat-curing adhesives. There are two types of thermosetting adhesives. One is room temperature curing type and the other is heat curing type, and the latter usually has a denser three-dimensional network structure and is said to be stronger than the room temperature curing type. The discussion in this paper is especially useful for heat-curing adhesives because they are widely used after being cured by heating to a temperature higher than room temperature. To evaluate the heat-curing adhesive strength, it is necessary to consider both the thermal stress generated during heat curing and external loads such as tensile stress.

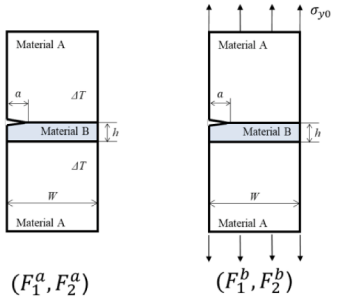

(a) ABA joint under uniform temperature change ΔT (b) ABA joint under remote tensile stress which is equal to equivalent stress σ_{y0}

Fig. 1. Butt joint named ABA joint in this paper under thermal loading compared to tensile loading assuming a fictitious crack length *"a"*. Note that equivalent stress $\sigma_{y0} = \frac{8G_AG_B\left(\eta_B^*-\eta_A^*\right)\Delta T}{G_A(\kappa_B-1)-G_B(\kappa_A-1)-2(G_A-G_B)}$ provides the same ISSF for (a), (b) when no crack. Here, Material A, B have elastic constants G_A, κ_A, G_B, κ_B and thermal expansion coefficients $\eta_m^* = \eta_m$(plane stress), $\eta_m^* = (1+\nu_m)\eta_m$(plane strain), $m = A, B$, $F_1 + iF_2 = (K_1 + iK_2)/\sigma_{y0}\sqrt{\pi a}$, $\sigma_y(r) + i\tau_{xy}(r) \to \frac{K_1+iK_2}{\sqrt{2\pi r}}\left(\frac{r}{2a^e}\right)^{i\varepsilon}$.

2. ISSF of ABA joint without crack under tension and thermal loading

Before discussing the SIF of an edge interface crack under thermal loading, in this Section 2, the Intensity the Singular Stress Field (ISSF) of ABA joint will be described for thermal loading. This is because the SIF of the edge crack in Fig. 2 should be discussed based on the double singularities before and after cracking as shown in the previous studies [28,29]. In the previous studies, Bogy pointed out the existence of logarithmic singularity in dissimilar bonded plates under surface traction without mentioning the equivalent tensile stress of the thermal loading [7]. Chen et al [21] explained that the stress distribution due to thermal loading can be expressed by the stress distribution under tension and the constant uniform stress without mentioning that the meaning of the constant stress value [11,12,30]. Therefore, in this Section 2, the interfacial stress distributions under tension and thermal loading will be indicated focusing on the difference of the singular stress distribution. Though the explanation, the value of the constant stress will be clarified to understand the edge interface crack problem [21,25].

Fig. 3(a) illustrates the interface stress $\sigma_y(r)$ of the ABA joint when $\alpha = 0.8, \beta = 0.3$ in comparison with the AB joint subjected to $\sigma_y^{\infty}(x)$. The remote tensile stress can be chosen as $\sigma_y^{\infty}(x) = \sigma_{y0}$, which will be defined later in Eq. (6) as shown in Fig. 3 (a) without losing generality. The singular stress distribution $\sigma_y(r)$ can be expressed in Eq. (1) at the interface edge.

$$\sigma_y(r) = \frac{K_\sigma}{r^{1-\lambda}} \text{ due to } \sigma_{y0}, K_\sigma = F_\sigma^* \sigma_{y0} h^{1-\lambda} \tag{1}$$

Here, K_σ is the intensity of the singular stress field (ISSF) and λ is the edge singularity index whose value is given by the characteristic equation of Eq. (2) [27]. The ISSF K_σ of the ABA joint under tension σ_{y0} in Fig. 3(a) discussed in Ref. [27] are indicated in Appendix A under arbitrary material combinations as $F_\sigma^* = K_\sigma/\sigma h^{1-\lambda}$.

$$\left[\sin^2\left(\frac{\pi}{2}\lambda\right) - \lambda^2\right]^2\beta^2 + 2\lambda^2\left[\sin^2\left(\frac{\pi}{2}\lambda\right) - \lambda^2\right]\alpha\beta + \lambda^2(\lambda^2-1)\alpha^2 + \frac{\sin^2(\lambda\pi)}{4} = 0 \tag{2}$$

In Eq. (2), Dundurs parameters α, β are determined from the material combination as follows [31].

$$\alpha = \frac{G_A(\kappa_B+1) - G_B(\kappa_A+1)}{G_A(\kappa_B+1) + G_B(\kappa_A+1)}, \beta = \frac{G_A(\kappa_B-1) - G_B(\kappa_A-1)}{G_A(\kappa_B+1) + G_B(\kappa_A+1)}, \tag{3}$$

$$\kappa_m = \begin{cases} (3-\nu_m)/(1+\nu_m) \text{(plane stress)} \\ 3-4\nu_m \text{(plane strain)} \end{cases}, (m = A, B) \tag{4}$$

Fig. 3(b) shows the stress distribution $\sigma_y(r)$ at the interface edge due to the thermal loading by cooling the plate's temperature uniformly as $\Delta T = T_0 < 0$. Fig. 3(b) is an example when $\alpha = 0.8, \beta = 0.3, T_0 = -100$ deg, and linear expansion coefficient ratio $\eta_A/\eta_B = 10$. To conform the constant term associated with the thermal loading, Fig. 3(c) shows the subtracted distribution of Fig. 3(b) from Fig. 3(a). As shown in Fig. 3(c), a constant interface stress distribution $\sigma_y^c(r) = \sigma_{y0}$ is confirmed as can be expressed $\sigma_y^c(r) = \sigma_y^a(r) - \sigma_y^b(r) = \sigma_{y0}$. The dashed line in Fig. 3(b) is the stress σ_y at the interface due to the uniform temperature change $\Delta T = -T_0 < 0$ subtracting the constant term $\sigma_y = \sigma_{y0}$ in Fig. 3(c).

From Fig. 3(c), it can be confirmed that the singular stress distribution under thermal loading in Fig. 3(b) at the interface end $\sigma_y(r)$ can be expressed in Eq. (5).

$$\sigma_y(r) = \frac{K_\sigma}{r^{1-\lambda}} + \sigma_{y0} \text{ due to } \Delta T \tag{5}$$

In other words, under the bad pair condition satisfying $\alpha(\alpha - 2\beta) > 0$ the power function type singular stress field $r^{1-\lambda}$ occurs in the case of the thermal load as well as in the case of the mechanical load causing $\sigma_y(r) \to \infty$ as $r \to 0$. The constant term σ_{y0} is known as the equivalent remote tensile stress that should be applied to the bimaterial plate (see Fig. 3(a)) to produce the same ISSF (see Fig. 3(b)). Under the remote tensile stress σ_{y0} defined in Eq. (6), the same intensity of the singular stress K_σ due to the uniform temperature change $\Delta T = -T_0 < 0$ can be obtained [21,25,30].

$$\sigma_{y0} = \frac{8G_AG_B\left(\eta_B^* - \eta_A^*\right)\Delta T}{G_A(\kappa_B-1) - G_B(\kappa_A-1) - 2(G_A - G_B)},$$

$$\eta_m^* = \begin{cases} \eta_m \text{ (plane stress)} \\ (1+\nu_m)\eta_m \text{(plane strain)} \end{cases} (m = A, B) \tag{6}$$

Here, G_A, G_B, are shear modulus, ν_A, ν_B are Poisson's ratio and η_A^*, η_B^* are thermal expansion coefficient of material A, B, respectively.

The singularity index $\lambda < 1$ obtained from Eq. (2) characterizes the presence of the singular stress in Fig. 3 in the following way.

1) When $\alpha(\alpha - 2\beta) > 0$ (Bad pair), $0 < \lambda < 1$.
2) When $\alpha(\alpha - 2\beta) = 0$ (Equal pair), $\lambda = 1$.
3) When $\alpha(\alpha - 2\beta) < 0$ (Good pair), $\lambda > 1$.

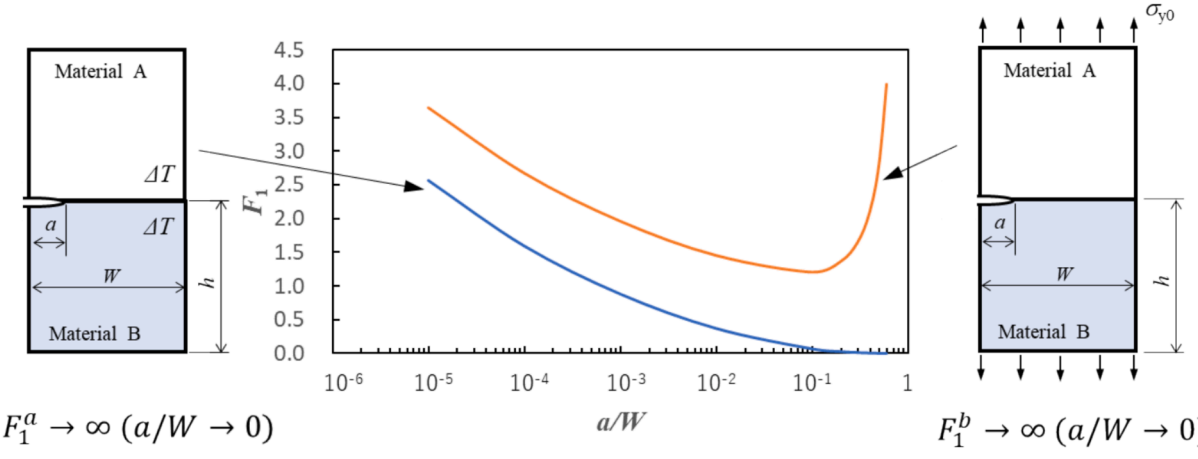

Fig. 2. Difference of the SIF between under thermal loading and under tensile loading in $F_1 - a/W$ relation in AB joint when $\alpha = 0.8, \beta = 0.3, \eta_A/\eta_B = 10, K_1 + iK_2 = (F_1 + iF_2)\sigma_{y0}\sqrt{\pi a}(1 + 2i\varepsilon), \sigma_y(r) + i\tau_{xy}(r) \to \frac{K_1 + iK_2}{\sqrt{2\pi r}}\left(\frac{r}{2a}\right)^{i\varepsilon}$, $r \to 0$ (r is a distance from the crack tip). Note that when no crack the ISSFs are equal. The AB joint in Fig. 2 can be regarded as ABA joint in Fig. 1 with $h/W \geq 1$.

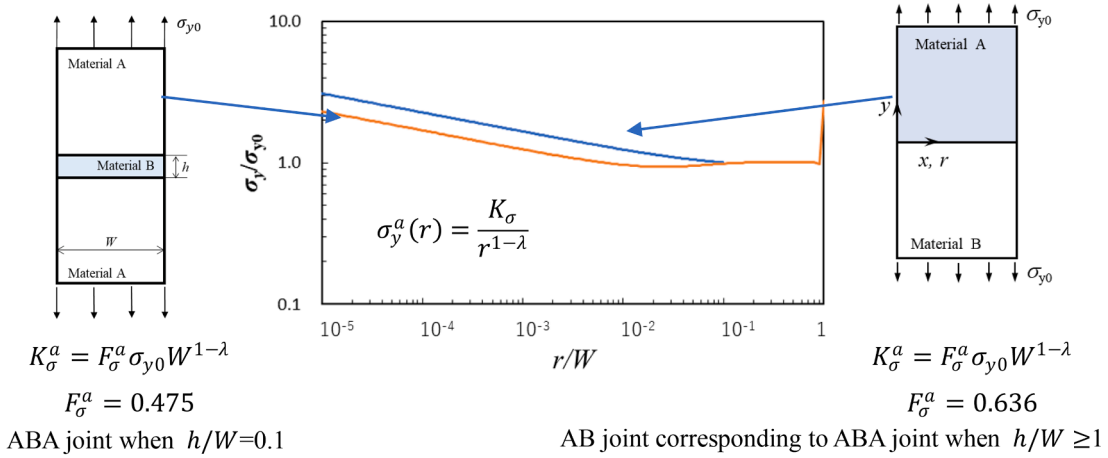

(a) Interface stress distributions $\sigma_y^a(r)$ due to remote tensile loading $\sigma_y^\infty(x) = \sigma_{y0}$ for ABA joint when h/W=0.1 and $h/W \geq 1.0$ which is corresponding to AB joint

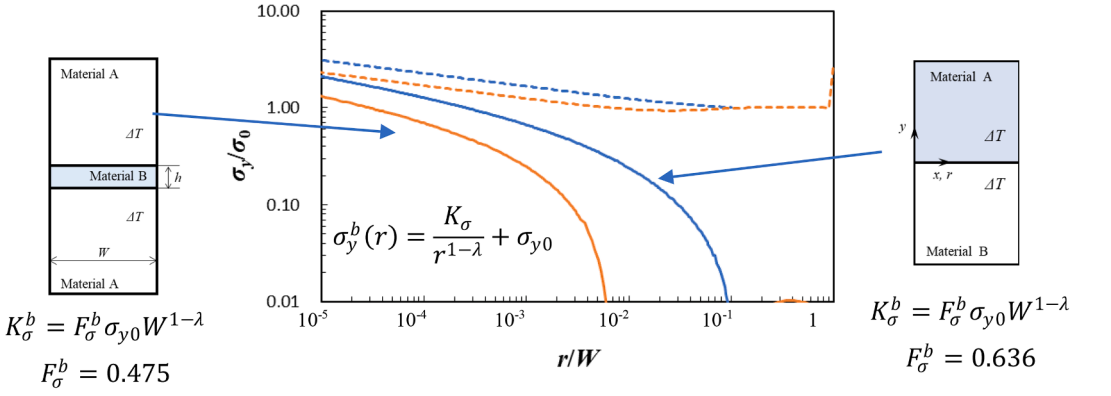

$$\sigma_{y0} = \frac{8G_A G_B(\eta_B^* - \eta_A^*)\Delta T}{G_A(\kappa_B - 1) - G_B(\kappa_A - 1) - 2(G_A - G_B)}, \qquad \eta_m^* = \begin{cases} \eta_m & \text{(plane stress)} \\ (1+\nu_m)\,\eta_m & \text{(plane strain)} \end{cases} (m = A, B)$$

(b) Interface stress distributions $\sigma_y^b(r)$ due to negative uniform temperature change $\Delta T = T_0 < 0$ for ABA joint when h/W=0.1 and $h/W \geq 1.0$ which is corresponding to AB joint

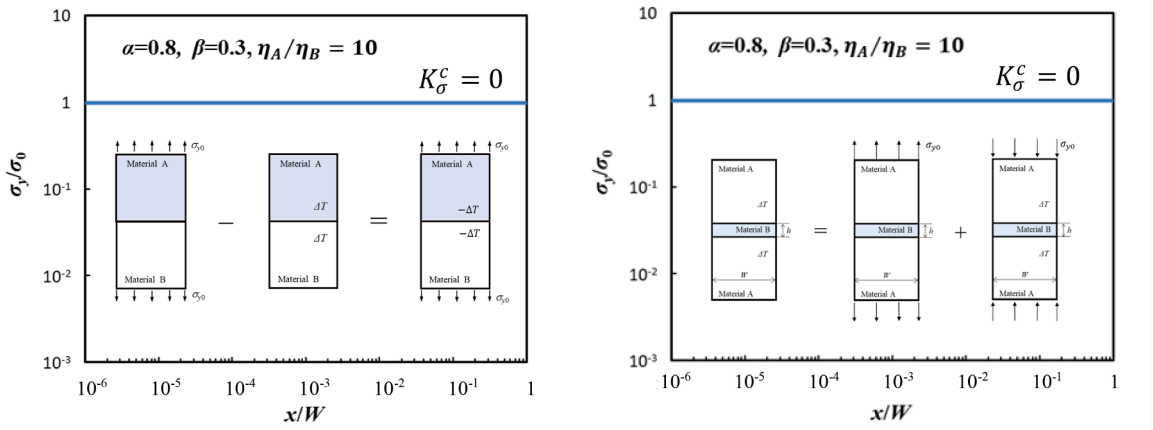

(c) Constant interface stress distribution $\sigma_y^c(r) = \sigma_{y0}$ obtained by subtracting Fig.3(b) from Fig.3(a) as $\sigma_y^c(r) = \sigma_y^a(r) - \sigma_y^b(r) = \sigma_{y0}$ for ABA joint when h/W=0.1 and $h/W \geq 1.0$ which is corresponding to AB joint

Fig. 3. Interface stress distribution $\sigma_y(r)$ under mechanical loading and thermal loading for ABA joint when $h/W = 0.1$ and $h/W \geq 1.0$ which is corresponding to AB joint under fixed material combination $\alpha = 0.8, \beta = 0.3$ obtained as $G_A/G_B = 10.93$, $\nu_A/\nu_B = 0.0314$, plane stress), $\Delta T = T_0 = -100$ deg, thermal expansion coefficient ratio $\eta_A/\eta_B = 10$.

Table 1
Behaviors of the interface stress $\sigma_y(r)$ when $r\to 0$ in Fig. 3 under mechanical loading and thermal loading.

Material combination	Under thermal loading	Under tensile loading
$\alpha(\alpha-2\beta)>0$ (Bad pair)	$\sigma_y(r)=\frac{K_\sigma}{r^{1-\lambda}}+\sigma_{y0}\to\infty\,(r\to 0)$	$\sigma_y(r)=\frac{K_\sigma}{r^{1-\lambda}}\to\infty\,(r\to 0)$
$\alpha(\alpha-2\beta)=0$ (Equal pair)	$\sigma_y(r)=k_\sigma\log(r)\to\infty\ (r\to 0)$ $(\alpha\neq 0)$	$\sigma_y(r)\to$finite $(r\to 0)$
$\alpha(\alpha-2\beta)<0$ (Good pair)	$\sigma_y(r)\to$finite $(r\to 0)$	$\sigma_y(r)\to 0\ (r\to 0)$

Table 1 summarizes the difference between the singular stress fields under mechanical loading and the one under thermal loading. The presence or absence of the interface stress singularity was discussed in the previous studies [12,25]. Table 1 summarizes the behaviors of the interface stress $\sigma_y(r)$ when $r\to 0$ in Fig. 3 under mechanical loading and thermal loading. The interface stress behavior varies depending on $\alpha(\alpha-2\beta)>0$, $\alpha(\alpha-2\beta)=0$, $\alpha(\alpha-2\beta)<0$. Note here that the ISSF K_σ due to mechanical load σ_{y0} in Eq. (1) and the ISSF K_σ due to thermal stress ΔT in Eq. (5) are equal since the constant term σ_{y0} in Eq. (5) does not affect the ISSF.

Fig. 4 illustrates the idea of the analysis method used later in Section 4. The stress distribution in Fig. 4(a) under thermal loading consists of the one under the tensile loading in Fig. 4(b) and the constant interface stress in Fig. 4(c). The ISSF solution in Fig. 4(b) was analyzed previously. As shown in Fig. 4(c), the uniform interface stress in Fig. 4(c) is expressed by the sum of the compressive remote loading and the thermal loading. In this study, the stress intensity factor of the edge crack in the butt joint under uniform temperature change will be discussed based on the superposition in Fig. 4. Accurate values of ISSFs $F_\sigma^*=K_\sigma/\sigma h^{1-\lambda}$ of ABA joints are indicated in Table A1 and Fig.A1 in Appendix A under arbitrary material combinations. Also, the usefulness of these results is indicated in Fig. A2 in Appendix A.

3. Analysis method of interfacial cracks under thermal load

3.1. Fictious crack method to analyze adhesive strength

The ABA joints are often used as a most fundamental testing method to evaluate adhesive strength. Suzuki [32] measured the adhesive strength of ABA joints by varying adhesive layer thicknesses stating that the maximum principal stress value at a distance δ from the surface can be used to predict the strength. Reedy-Guess [33,34], Reedy [35] and Mintzas-Nowell [36] focused on the interface edge singular field stating that the generalized stress intensity factor (ISSF) to evaluate the strength. Noda et al. [37] analyzed the intensity of the singular stress fields (ISSF) at the end of ABA joint interface controlling the strength by varying the material combination and adhesive layer thickness stating that the ISSF controls the strength. Furthermore, they explained the stress intensity factor (SIF) of an assumed fictitious interface crack is also useful since the adhesive strength can be expressed as a constant value of the SIF [37]. This is because the SIF of the assumed edge crack is controlled by the ISSF of the singular stress field at the interface end [28,29,38].

To evaluate the adhesive strength based on the singular field at the edge of the interface, the ISSF method and the fictitious crack method, which assumes an interfacial crack at the interface end as shown in Fig. 1, have been proposed [37]. In the ISSF method, the adhesive strength is evaluated using the parameter K_σ related to the normal stress σ_y at the interface. On the other hand, the strength evaluation method using a fictitious crack investigated in this study uses the SIFs K_1, K_2 of the interfacial crack as substitute parameters for the strength of the singular field K_σ at the edge of the interface. Since not only K_1 related to σ_y but also K_2 related to shear stress τ_{xy} can be obtained, there is an advantage that the mechanical state of interfacial failure can be intuitively understood.

3.2. Proportional method to analyze thermal interface stress intensity factors

Fig. 5 shows a butt joint with an edge interface crack subjected to uniform temperature change ΔT, which is the target problem in this study. In the FEM analysis, a uniform temperature change ΔT is applied to the entire element in Fig. 4 considering elastic modulus and linear expansion coefficient. Then, the stress value at the crack tip is calculated. In a similar way, an interface edge crack under heat flow may be solved after analyzing temperature distribution [39]. Since the singular field appears at the interface end of the bonded plate without crack, the discussion in Section 2 must be useful for heat flow problems. In this study, the SIF of the interface crack under uniform temperature change ΔT is focused by applying the proportional method [28,29,38]. As shown in the preceding papers as well as the following explanation in Sections 3 and 4, the proportional method may provide exact solutions [25,28,29,38].

In the method, stress values at the crack tip node are used and a stress intensity factor is determined by the ratio of the crack tip stress values between an unknown problem in Fig. 5 and the reference problem in Fig. 6. In this study, the definition of stress intensity factor is expressed as follows based on the interface crack length $2a^*$.

$$\sigma_y(r)+\ i\tau_{xy}(r)\to\frac{K_1+i\,K_2}{\sqrt{2\pi r}}\left(\frac{r}{2a^*}\right)^{i\varepsilon},\ (r\to 0) \tag{7}$$

The method gives the singular stress field equal to the unknown problem by adjusting load stress T and S of the reference problem whose stress intensity factor is already-known. The single interface crack in a bonded semi-infinite plate subjected to the tension T and shear S is selected as the reference problem because the interface crack tip is always mixed mode state. The stress values at the interface crack tip node calculated by FEM in the reference problem under the tensile stress $T=1$ $(S=0)$ or shear stress $S=1$ $(T=0)$ are written by $\sigma_{y0,FEM}^{T=1*}$, $\tau_{xy0,FEM}^{T=1*}$ and $\sigma_{y0,FEM}^{S=1*}$, $\tau_{xy0,FEM}^{S=1*}$, respectively in Fig. 5. The crack tip stress values of the unknown problem under the uniform temperature change in Fig. 5 are also denoted by $\sigma_{y0,FEM}$, $\tau_{xy0,FEM}$. By using the same crack tip stress condition between the reference and the unknown problems, that is, $\sigma_{y0,FEM}=\sigma_{y0,FEM}^*$ and $\tau_{xy0,FEM}=\tau_{xy0,FEM}^*$, the external loading stress T and S in the reference problem can be determined from the next expression (8).

$$T=\frac{\sigma_{y0,FEM}\cdot\tau_{xy0,FEM}^{S=1*}-\sigma_{y0,FEM}^{S=1*}\cdot\tau_{xy0,FEM}}{\sigma_{y0,FEM}^{T=1*}\cdot\tau_{xy0,FEM}^{S=1*}-\sigma_{y0,FEM}^{S=1*}\cdot\tau_{xy0,FEM}^{T=1*}},\qquad S=\frac{\sigma_{y0,FEM}^{T=1*}\cdot\tau_{xy0,FEM}-\sigma_{y0,FEM}\cdot\tau_{xy0,FEM}^{T=1*}}{\sigma_{y0,FEM}^{T=1*}\cdot\tau_{xy0,FEM}^{S=1*}-\sigma_{y0,FEM}^{S=1*}\cdot\tau_{xy0,FEM}^{T=1*}} \tag{8}$$

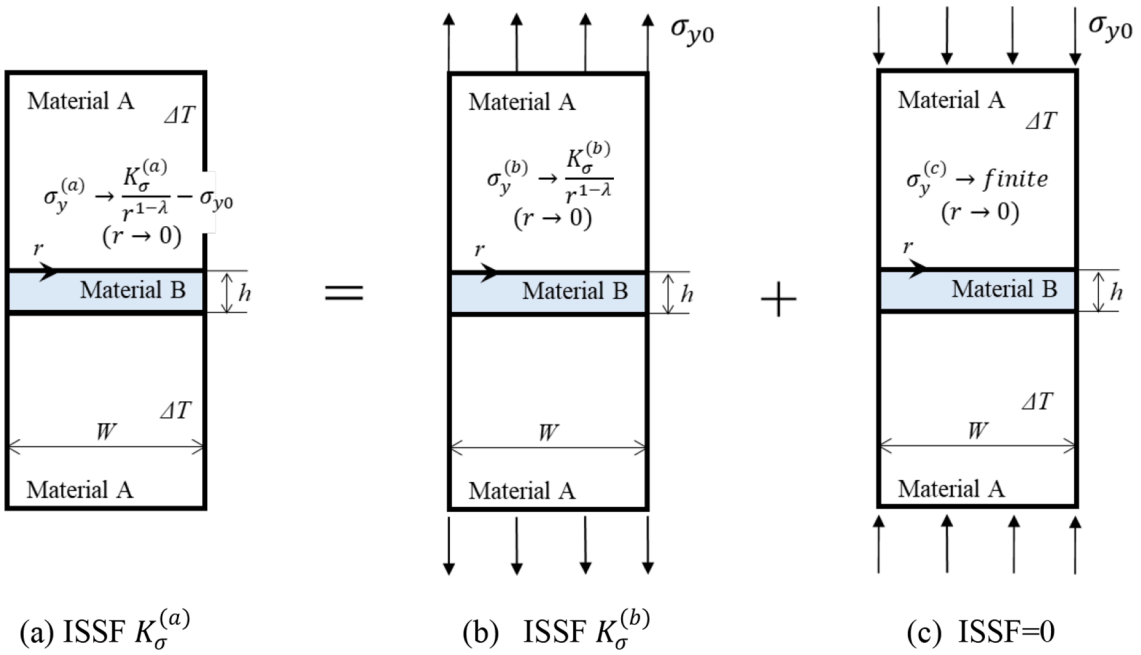

Fig. 4. (a) Singular interface stress due to uniform thermal loading $\Delta T = T_0 < 0$ can be expressed by superposing (b) tensile loading and (c) constant interface stress when $\alpha(\alpha - 2\beta) > 0$. The constant interface stress in Fig. 3(c) can be obtained from compressive σ_{y0} and $\Delta T = T_0 < 0$.

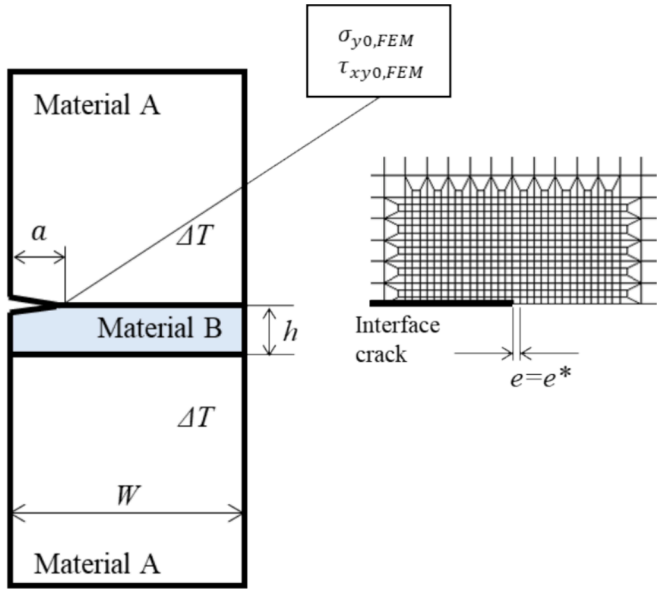

Fig. 5. Unknown problem for an edge interface crack in bi-material rectangular plate subjected to uniform temperature change ΔT. The stress values at the crack tip $\sigma_{y0,FEM}$, $\tau_{xy0,FEM}$ are calculated by FEM considering the elastic modulus G_A, ν_A, G_B, ν_B and thermal expansion coefficients η_A, η_B.

From the loading stresses T and S obtained by Eq. (8), the stress intensity factor of the interface crack in the reference problem in Fig. 6 can be evaluated by Eq. (9).

$$K_1^* + iK_2^* = (T + iS)\sqrt{\pi a^*}(1 + 2i\varepsilon),$$
$$\varepsilon = \frac{1}{2\pi}\ln\left[\left(\frac{\kappa_A}{G_B} + \frac{1}{G_B}\right) \Big/ \left(\frac{\kappa_B}{G_B} + \frac{1}{G_A}\right)\right] \tag{9}$$

Here, ε is the oscillation singular index, $\kappa_m = 3 - 4\nu_m$ (plane strain), $(3 - \nu_m)/(1 + \nu_m)$ (plane stress), $(m = \mathrm{A}, \mathrm{B})$. Because the stress intensity factor of Eq. (9) is equal to that of the unknown problem, the stress intensity factors of the unknown problem in Fig. 5 can be obtained as

$$K_1 = K_1^*, \quad K_2 = K_2^* \tag{10}$$

From $K_1 = K_1^*$, $K_2 = K_2^*$, (T, S) in Eq. (8) can be regarded as dimensionless SIFs (F_1, F_2) of unknown problem (see Eq. (11)). It is noted that in the proportional method the finite element models of the reference and the unknown problems have the same crack length and the same FEM mesh pattern near the interface crack tip [25,28,29,38], $a = a^*$ and $e = e^*$. The detail of the accuracy discussion can be found in previous papers under mechanical loading [28,29,38]. The proportional method is useful for analyzing interface cracks by providing mesh-independent interface SIFs F_1, F_2 efficiently. Since those FEM results are mesh-independent, the obtained SIFs K_1, K_2 can be regarded as the exact solution by using the exact reference solution in the bonded

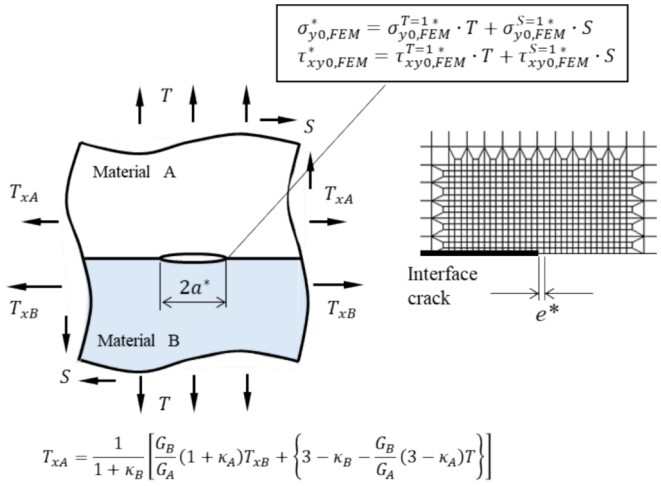

Fig. 6. Reference problem for an interface crack in a bonded semi-infinite plate subjected to tension T and shear S.

Table 2
Mesh-independence of F_1, F_2 obtained by the proportional method when $h/W = 0.1$ in Fig. 5 [$K_1 + iK_2 = (F_1 + iF_2)\sigma_{y0}\sqrt{\pi a}(1 + 2i\varepsilon)$, α=0.8, β=0.3, $a/W = 10^{-5}$ and $a/W = 0.1$].

h/W	a/W	e/a	Thermal loading		Tension	
			F_1	F_2	F_1	F_2
0.1	10^{-5}	$(3^{-6})/11$	1.643003	−0.2851651	2.725190	−0.230368
		$(3^{-7})/11$	1.642920	−0.2853527	2.725152	−0.230969
		$(3^{-8})/11$	1.643179	−0.2853674	2.724885	−0.230956
0.1	0.1	$(3^{-6})/11$	−0.0305951	−0.0757925	0.887870	−0.100019
		$(3^{-7})/11$	−0.0306005	−0.0757973	0.887860	−0.100019
		$(3^{-8})/11$	−0.0306041	−0.0758045	0.887899	−0.099987

Table 3
Confirmation of the thermal SIFs F_1, F_2 defined from $K_1 + iK_2 = (F_1 + iF_2)\sigma_{y0}\sqrt{\pi a}(1 + 2i\varepsilon)$ are controlled by α, β by taking an example when $\alpha = 0.8$, β=0.3 and $h/W = 0.1$, $a/W = 10^{-5}$ in Fig. 4.

Analysis conditions		Case 1 (Plane stress)	Case 2 (Plane stress)	Case 3 (Plane strain)	Case 4 (Plane strain)
Shear modulus [MPa]	G_A	496.524	4878.049	99.999	3998.612
	G_B	45.426	453.515	9.091	363.625
Poisson's ratio	ν_A	0.007	0.025	0.000011	0.000347
	ν_B	0.223	0.225	0.181819	0.181844
Thermal expansion [1/K]	η_A	10	10	5	3
	η_B	1	100	2	20
Temperature change [K]	ΔT	100	100	100	100
Equivalent stress (Eq.6)	σ_{y0}	450,000	−45000000	26,364	−8254337
Normalized SIF	F_1	1.6431	1.6431	1.6431	1.6431
	F_2	−0.2854	−0.2854	−0.2854	−0.2854

infinite plate $K_1 + iK_2 = (T + iS)\sqrt{\pi a}(1 + 2i\varepsilon)$. In Table 2, several examples are indicated.

3.3. Effect of material combination on the thermal interface stress intensity factors

In this study, the dimensionless stress intensity factors F_1 and F_2 defined in Eq. (11) will be used to discuss ABA joints by applying the proportional method in section 3.1.

$$K_1 + iK_2 = (F_1 + iF_2)\sigma_{y0}\sqrt{\pi a}(1 + 2i\varepsilon) \tag{11}$$

In Eq. (11), the equivalent stress is defined by Eq. (6).

The thermal stress intensity factor (SIF) varies depending on the temperature change ΔT, Dundurs parameter α, β, thermal expansion coefficient ratio η_A/η_B, and relative crack length a/W. Table 3 shows the values of F_1 and F_2 for an edge interfacial crack under fixed $\alpha = 0.8$, β=0.3 and fixed geometry $h/W = 0.1$, $a/W = 10^{-5}$ by varying material constants. From Table 3, it can be seen that even if the material constants are different, the values of F_1, F_2 are the same. This is because Dundurs parameters α, β control F_1, F_2.

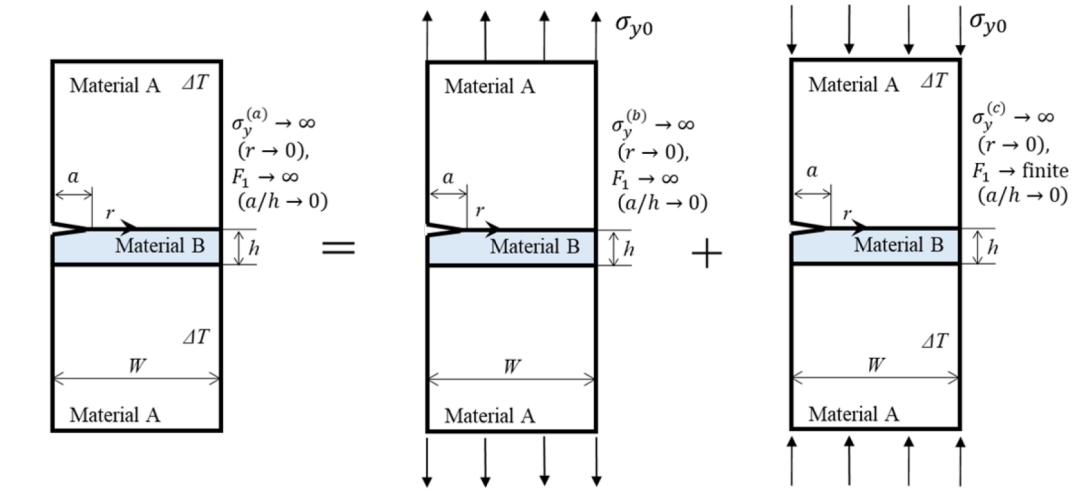

Fig. 7. (a) Singular interface stress of ABA joint due to uniform thermal loading $\Delta T = T_0 < 0$ which can be expressed by superposing (b) tensile loading and (c) constant interface stress when $\alpha(\alpha - 2\beta) > 0$. The constant interface stress in Fig. 7(c) can be obtained from compressive σ_{y0} and $\Delta T = T_0 < 0$, [$K_1 + iK_2 = (F_1 + iF_2)\sigma_{y0}\sqrt{\pi a}(1 + 2i\varepsilon)$].

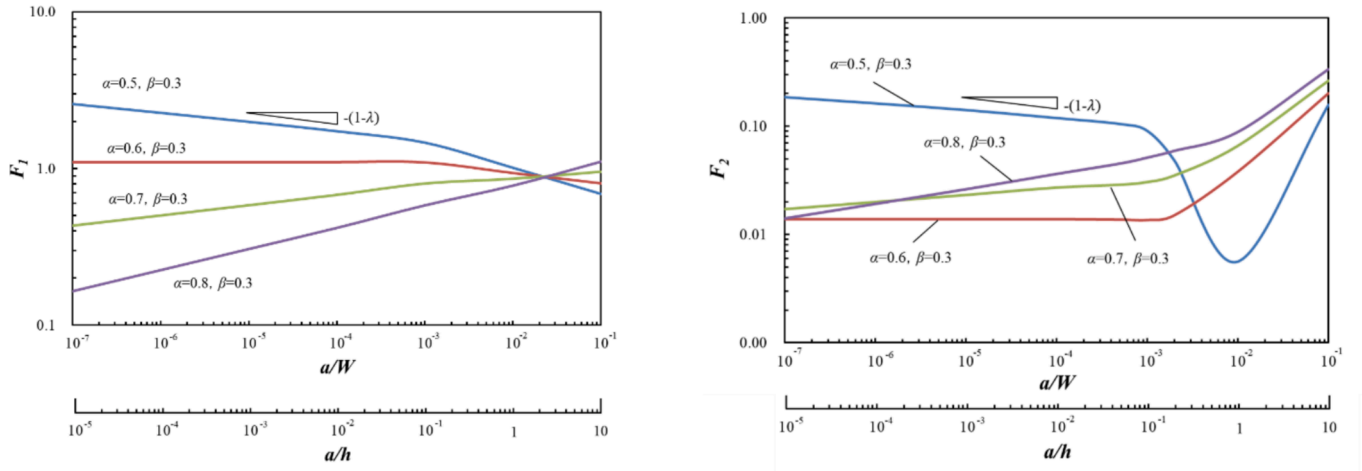

Fig. 8. F_1, F_2 $-$ a/W relation for ABA joint in Fig. 7 (b) showing that $\ln[F_1/(a/W)] \approx -(1-\lambda)$, $\ln[F_2/(a/W)] \approx -(1-\lambda)$ when $a/W \leq 10^{-1}$, λ= singularity index, $h/W = 0.01$ $[K_1 + iK_2 = (F_1 + iF_2)\sigma_{y0}\sqrt{\pi a}(1 + 2i\varepsilon)]$.

4. Stress intensity factor of an interface edge crack in butt joint under tensile loading in Fig. 7 (b)

As shown in Section 2 (see Fig. 2 and Fig. 3), the interfacial stress distribution due to uniform temperature change in the ABA joints without crack (Fig. 3(a)) can be composed of the tensile load problem (Fig. 3(b)) and the uniform stress problem (Fig. 3(c)). In this study, the problem of interfacial edge cracking in the ABA joints due to thermal stress (Fig. 7 (a)) is investigated by superimposing Fig. 7(b) and 7(c). In this Section, the effect of the crack length a/W and bondline thickness h/W on the SIF of the interface edge crack under tensile load in Fig. 7(b).

4.1. Effect of crack length a/W and bondline thickness h/W on F_1, F_2 under tension

The SIF in Fig. 1(b) is affected by crack length a/W and adhesive layer thickness h/W. In this section, the effect of those geometry on the SIF in Fig. 1 will be investigated to understand the edge interface crack in ABA joint.

Fig. 8 shows F_1, F_2 $-$ a/W relation in a log–log diagram for ABA joint in Fig. 7(b). The crack length "a" is changed widely in a range $a/W = 10^{-7} \sim 10^{-1}$. The adhesive layer thickness h is set to be relatively larger than "a" as $a/h = 0.1$ and indicated in the second x-axis of a/h. The material combinations are $\alpha = 0.5 \sim 0.8$ with fixed $\beta = 0.3$. As shown in Fig. 8, when $a/W \leq 10^{-3}$ or $a/h \leq 0.1$, it can be seen F_1, F_2 change linearly in a log–log diagram with respect to a/W and the slope agrees with $-(1-\lambda)$ by using the singularity index λ. This is because the ISSF K_σ is proportional to $h^{1-\lambda}$ as shown in Eq. (6), $K_\sigma = F^*_\sigma \sigma_{y0} h^{1-\lambda}$ [27].

Fig. 9 shows F_1, F_2 $-h/W$ relation in a log–log diagram for ABA joint in Fig. 7(b). The adhesive layer thickness h is changed widely in the range $h/W = 0.002 \sim \infty$. The relative crack length is set to be relatively smaller than h as $a/h = 0.1$. The material combinations are $\alpha = 0.5 \sim 0.8$ with fixed $\beta = 0.3$. As shown in Fig. 9, when $h/W \leq 0.1$, F_1, F_2 change linearly in a log–log diagram with respect to the adhesive layer thickness h/W, and the slope agrees with $-(1-\lambda)$ by using the singularity index λ. This is because the ISSF K_σ is proportional to $h^{1-\lambda}$ as shown in Eq. (6), $K_\sigma = F^*_\sigma \sigma_{y0} h^{1-\lambda}$ [27]. On the other hand, when the adhesive layer thickness is $h/W \geq 1$, F_1, F_2 are constant and independent of h.

4.2. Definition of SIF for an edge interface crack in butt joint under tension

From Figs. 8 and 9, it was clarified that F_1, F_2 change linearly in a log–log diagram with respect to a/W, and h/W. Then, the slope agrees with $-(1-\lambda)$ by using the singularity index λ. In previous studies [25,28,29], the SIF of the edge interface crack in AB joint under tension

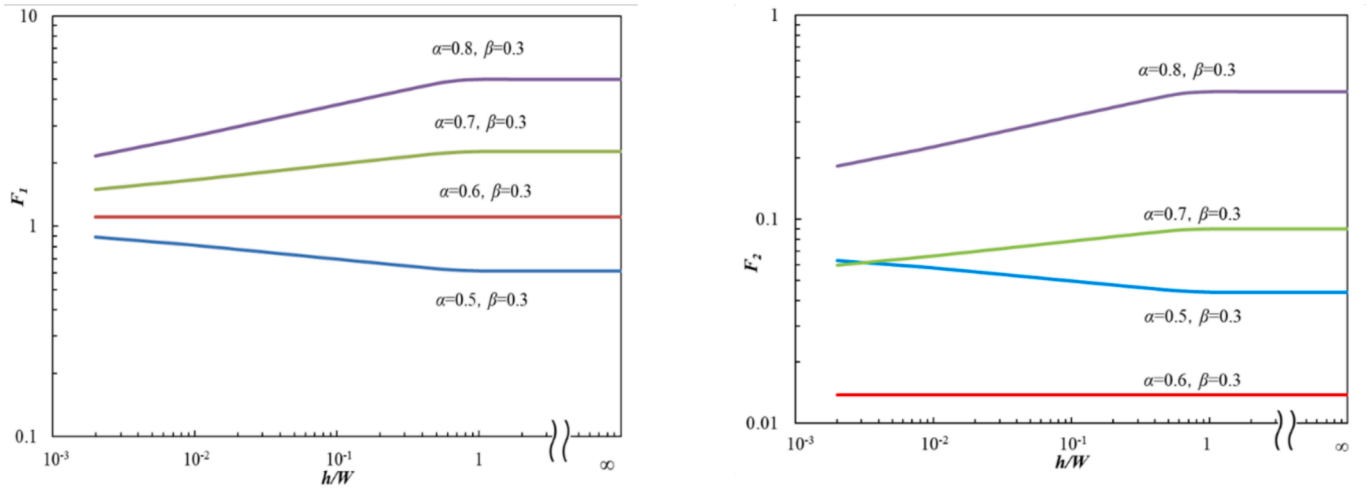

Fig. 9. F_1, F_2 $-h/W$ relation for ABA joint in Fig. 7 (b) showing that $\ln[F_1/(h/W)] \approx -(1-\lambda)$, $\ln[F_2/(h/W)] \approx -(1-\lambda)$ when $h/W \leq 10^{-1}$, λ= singularity index $[K_1 + iK_2 = (F_1 + iF_2)\sigma_{y0}\sqrt{\pi a}(1 + 2i\varepsilon)]$.

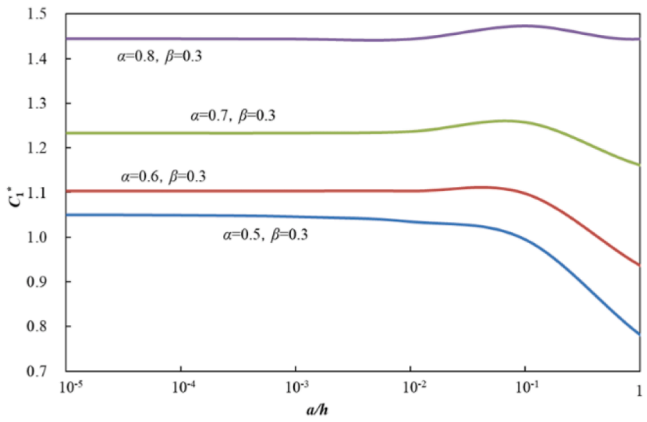

(a) $C_1^* = F_1/(h/a)^{1-\lambda}$ vs a/h

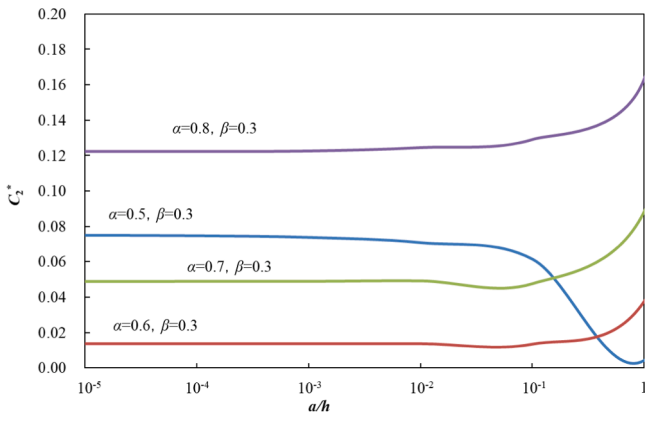

(b) $C_2^* = F_2/(h/a)^{1-\lambda}$ vs a/h

Fig. 10. $C_1{}^*$, $C_2{}^*$ $- a/h$ relation for ABA joint in Fig. 7 (b) showing that $C_1{}^*$, $C_2{}^*$ = constant when $a/h \leq 0.1$, $h/W = 0.01, \alpha = 0.5 \sim 0.8$, $\beta = 0.3$, $K_1 + iK_2 = (F_1 + iF_2)\sigma_{y0}\sqrt{\pi a}(1 + 2i\varepsilon), F_1 = C_1^*(h/a)^{1-\lambda}, F_2 = C_2^*(h/a)^{1-\lambda}$

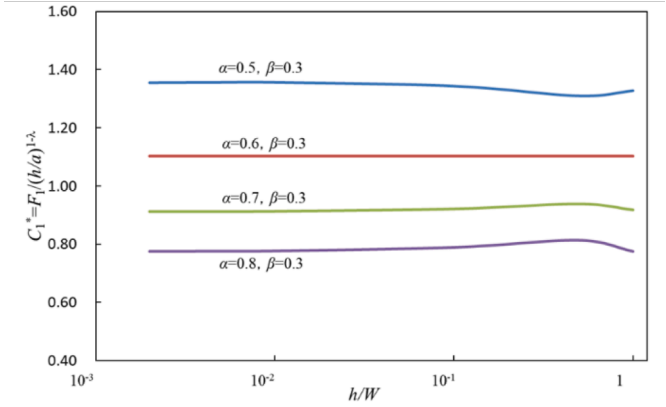

(a) $C_1{}^* = F_1/(h/a)^{1-\lambda}$ vs h/W

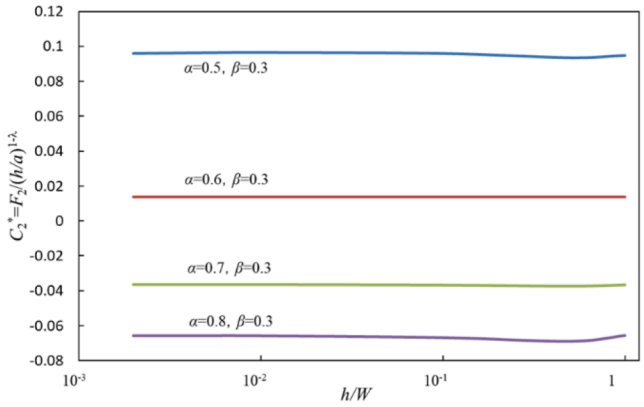

(b) $C_2{}^* = F_1/(h/a)^{1-\lambda}$ vs h/W

Fig. 11. $C_1{}^*$, $C_2{}^*$ $- h/W$ relation for ABA joint in Fig, 7 (b) when $h/W \leq 0.1$ showing that $C_1{}^*, C_2{}^*$ = const. when $a/h \leq 0.1$, $\alpha = 0.5 \sim 0.8$, $\beta = 0.3$, $K_1 + iK_2 = (F_1 + iF_2)\sigma_{y0}\sqrt{\pi a}(1 + 2i\varepsilon), F_1 = C_1^*(h/a)^{1-\lambda}, F_2 = C_2^*(h/a)^{1-\lambda}$

is expressed in the form $F_1 = C_1(W/a)^{1-\lambda}$, $F_2 = C_2(W/a)^{1-\lambda}$ indicating that the coefficients C_1, C_2 are constant when $a/W \leq 0.01$. Considering this, F_1, F_2 of the edge interface crack in ABA joint under tension is defined in the following form based on the adhesive layer thickness h.

$$\begin{aligned} &K_1 + iK_2 = (F_1 + iF_2)\sigma_{y0}\sqrt{\pi a}(1 + 2i\varepsilon), \\ &F_1 = C_1^*(h/a)^{1-\lambda}, \\ &F_2 = C_2^*(h/a)^{1-\lambda} \end{aligned} \tag{12}$$

Fig. 10 shows $C_1{}^*$, $C_2{}^*$ $- a/h$ relation for ABA joint in Fig. 7(b) when the bondline thickness h is fixed as $h/W = 0.01$ by taking example when $\alpha = 0.5 \sim 0.8$, $\beta = 0.3$. Fig. 10 shows that $C_1{}^*$, $C_2{}^*$ = constant when the crack length is relatively smaller as $a/h \leq 0.1$.

Next, Fig. 11 shows $C_1{}^*$, $C_2{}^*$ $- h/W$ relation for ABA joint in Fig, 7(b) when $a/h \leq 0.1$ by taking example when $\alpha = 0.5 \sim 0.8$, $\beta = 0.3$. From Fig. 11, it is seen that $C_1{}^*$, $C_2{}^*$ are insensitive of h/W, and especially when $h/W \leq 0.1$, $C_1{}^*$, $C_2{}^*$ = constant. This is practically important because usually the adhesive layer thickness is in the range $h/W \leq 0.1$. By using the constant value of $C_1{}^*$, $C_2{}^*$, it may be concluded that the SIF of the interface edge cracks in ABA joints can be expressed accurately to the three digits when $a/h \leq 0.1$, $h/W \leq 0.1$. This is because the SIF of a fictitious crack is controlled by the constant ISSF defined in $F_\sigma^* = K_\sigma/(\sigma h^{1-\lambda})$ [27]. Since a useful SIF expression defined in Eq. (12) is available when $a/h \leq 0.1$ and $h/W \leq 0.1$, accurate values of $C_1{}^*$, $C_2{}^*$ are indicated in Table B1 in Appendix B.

When $h/W \geq 1$, F_1, F_2 of the edge interface crack in in ABA joint are independent of the adhesive layer thickness h, so the SIF should be defined as follows based on the joint width W.

$$\begin{aligned} &K_1 + iK_2 = (F_1 + iF_2)\sigma_{y0}\sqrt{\pi a}(1 + 2i\varepsilon), \\ &F_1 = C_1(W/a)^{1-\lambda}, \\ &F_2 = C_2(W/a)^{1-\lambda} \end{aligned} \tag{13}$$

The coefficients C_1, C_2 in Eq. (13) are constant when $h/W \geq 1$ because the ISSF controlling the SIF defined as $F_\sigma = K_\sigma/(\sigma W^{1-\lambda})$ is constant when $h/W \geq 1$ [27]. Since a useful expression defined in Eq. (13) is also available when $h/W \geq 1$, accurate values of C_1, C_2 are also indicated in Table B2 in Appendix B.

4.3. Values of coefficients C_1^*, C_2^* under arbitrary material combinations

Fig. 12 shows the coefficients C_1^*, C_2^* for arbitrary material combinations α, β with $\alpha \geq 0$. Note that as shown in Fig. 13 practical material combinations are in the range $\alpha \geq 0$ and metal/resin combinations are in the range $0.7 \leq \alpha$, $0 \leq \beta \leq 0.3$. The adhesive layer thickness is

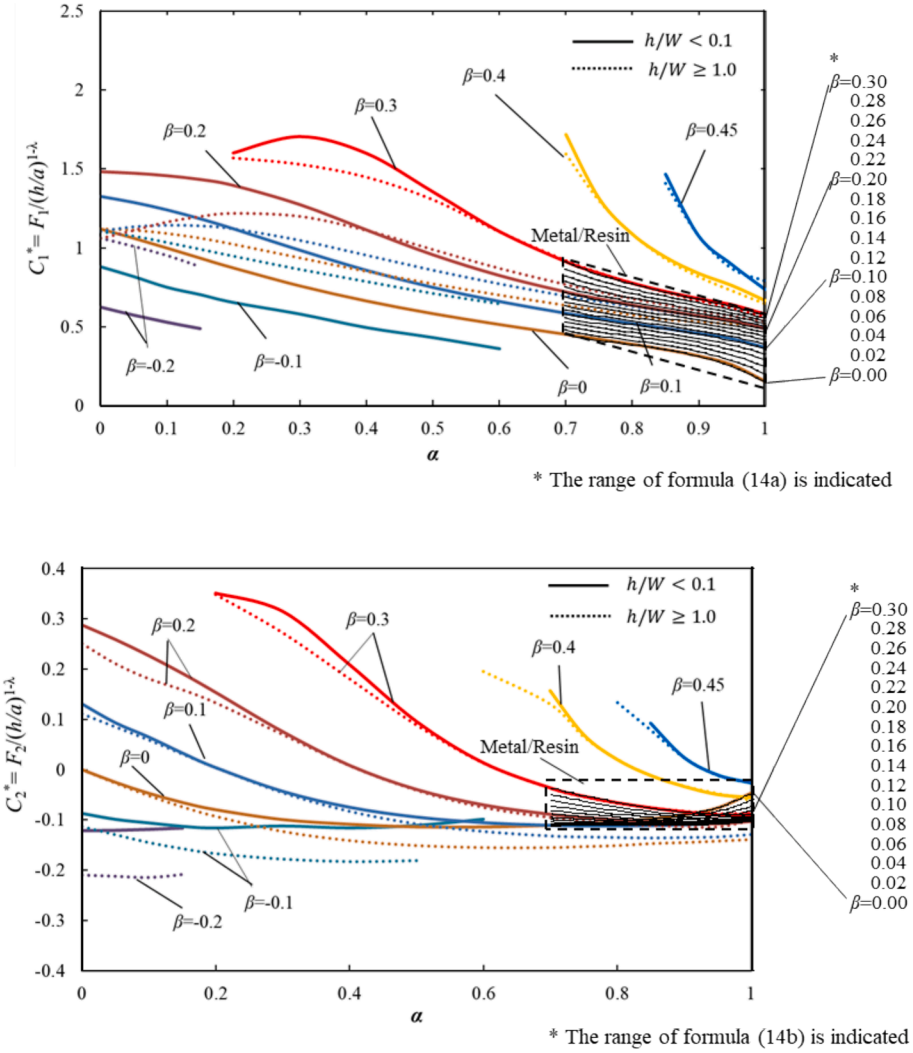

Fig. 12. Values of C_1^*, C_2^* in $K_1+iK_2=(F_1+iF_2)\sigma_{y0}\sqrt{\pi a}(1+2i\varepsilon)$ with $F_1=C_1^*(h/a)^{1-\lambda}+D_1^*$, $F_2=C_2^*(h/a)^{1-\lambda}+D_2^*$ having more than three digits accuracy for ABA joint in Fig. 7(b) when in the range $a/h\le 0.1$ and $h/W\le 0.1$ in comparison with values of C_1, C_2 in $K_1+iK_2=(F_1+iF_2)\sigma_{y0}\sqrt{\pi a}(1+2i\varepsilon)$ with $F_1=C_1(W/a)^{1-\lambda}+D_1^*$, $F_2=C_2(W/a)^{1-\lambda}+D_2^*$ having more than three digits accuracy for ABA joint in Fig. 7(b) when $h/W\ge 1$ (=AB joint) under arbitrary material combinations practically used $0\le\alpha\le 1$.

usually $h/W\le 0.1$. Since a useful expression defined by Eq. (13) is also available when $h/W\ge 1$, the values of the coefficients C_1, C_2 are also indicated by dashed lines (exact numbers are given in Appendix B). Comparison between the values of C_1^*, C_2^* shown by the solid line and the values of C_1, C_2 shown by the dotted line shows that under many practical material combinations (see Fig. 13) the effect of h/W is small. For readers' convenience, regarding Metal/resin combination in the range $0.7\le\alpha$, $0\le\beta\le 0.3$, the following formulas for calculating C_1^*, C_2^* are provided by applying the least square method.

When $0.7\le\alpha$, $0\le\beta\le 0.3$ (Metal/resin combination):

$$C_1^*=7.5609-59.501\beta+283.54\beta^2-304.73\beta^3$$
$$+[-26.082+236.42\beta-1105.3\beta^2+1303\beta^3]\alpha$$
$$+[32.28-304.94\beta+1420.1\beta^2-1770.3\beta^3]\alpha^2$$
$$+[-13.6+130.74\beta-605.55\beta^2+781.47\beta^3]\alpha^3 \quad (14a)$$

(less than 2.4 % error and less than almost 1 % error in most cases).

When $0.7\le\alpha$, $0\le\beta\le 0.3$ (Metal/resin combination):

$$C_2^*=-2.1157+22.214\beta-108.65\beta^2+201.93\beta^3$$
$$+[7.6267-83.539\beta+409.82\beta^2-726.91\beta^3]\alpha$$
$$+[-9.7143+104.89\beta-512.77\beta^2+881.29\beta^3]\alpha^2$$
$$+[4.1556-44.297\beta+214.45\beta^2-359.27\beta^3]\alpha^3 \quad (14b)$$

(less than 2.4 % error and less than almost 1 % error in most cases).

5. Stress intensity factor of an edge interface crack in ABA joint caused by constant term associated with thermal stress

When thermal load ΔT and compressive load σ_{y0} are applied at the same time as shown in Fig. 7(c), the adhesive interface has a uniform stress distribution. Under this condition, Fig. 14 shows D_1^*, D_2^*-a/h relation. Here, the SIF is defined in Eq. (15) when the material combinations $\alpha=0.5$, 0.7, 0.8, β=0.3, h/W=0.01. Fig. 14 shows that D_1^*, D_2^*

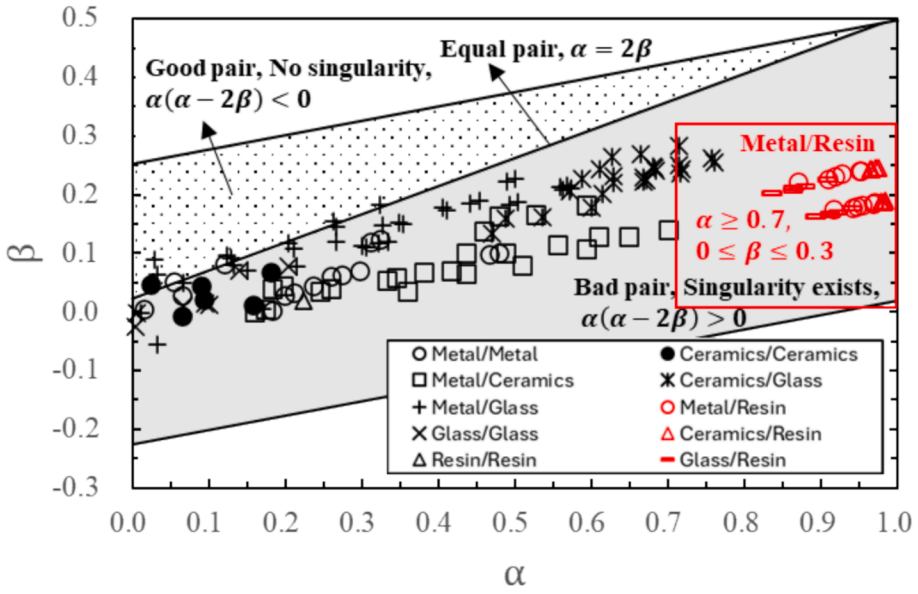

Fig. 13. Dundurs composite parameters for several engineering materials.

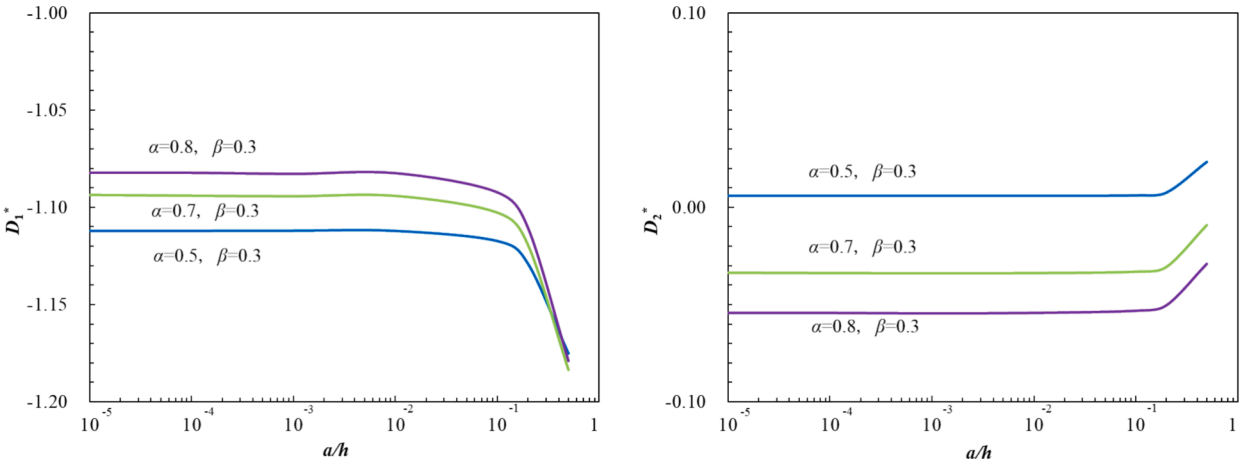

Fig. 14. ${D_1}^*, {D_2}^* - a/h$ relation for ABA joint in Fig. 7 (c) showing that ${D_1}^*, {D_2}^* =$ constant when $a/h \leq 0.1$ when $h/W = 0.01$, $\alpha = 0.5 \sim 0.8$, $\beta = 0.3, K_1 + iK_2 = ({D_1}^* + i{D_2}^*)\sigma_{y0}\sqrt{\pi a}(1+2i\varepsilon)$.

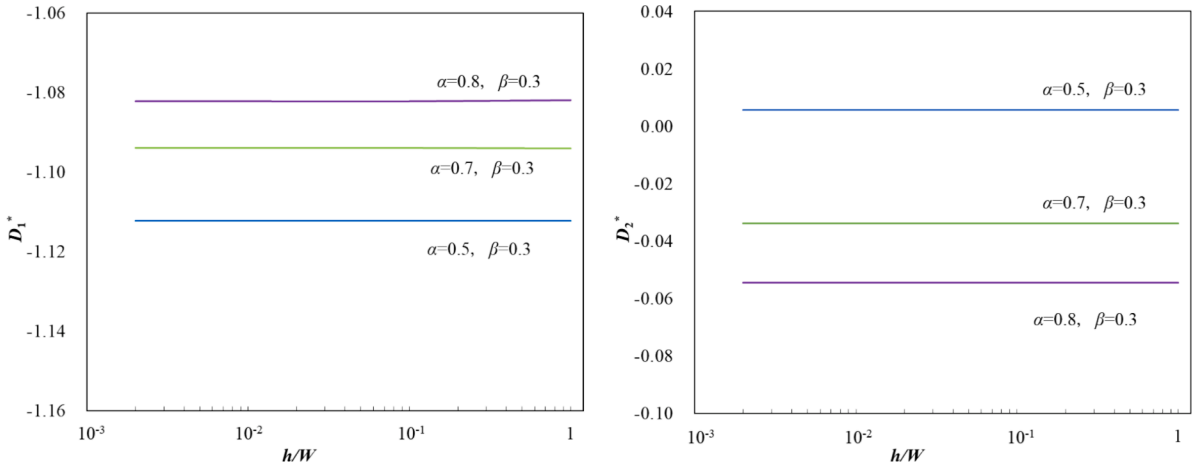

Fig. 15. ${D_1}^*, {D_2}^* - h/W$ relation in Fig. 7(c) for ABA joint showing that D_1^*, D_2^*=const. when $h/W \leq 1.0$, $\alpha = 0.5 \sim 0.8$, $\beta = 0.3$, $K_1 + iK_2 = \left(D_1^* + iD_2^*\right)\sigma_{y0}\sqrt{\pi a}(1+2i\varepsilon), \sigma_{y0} = \frac{8G_AG_B\left(\eta_B^*-\eta_A^*\right)\Delta T}{G_A(\kappa_B-1)-G_B(\kappa_A-1)-2(G_A-G_B)}, \eta_m^* = \begin{cases} \eta_m & (\textit{plane stress}) \\ (1+\nu_m)\,\eta_m & (\textit{plane strain}) \end{cases}, (m = \mathrm{A}, \mathrm{B})$

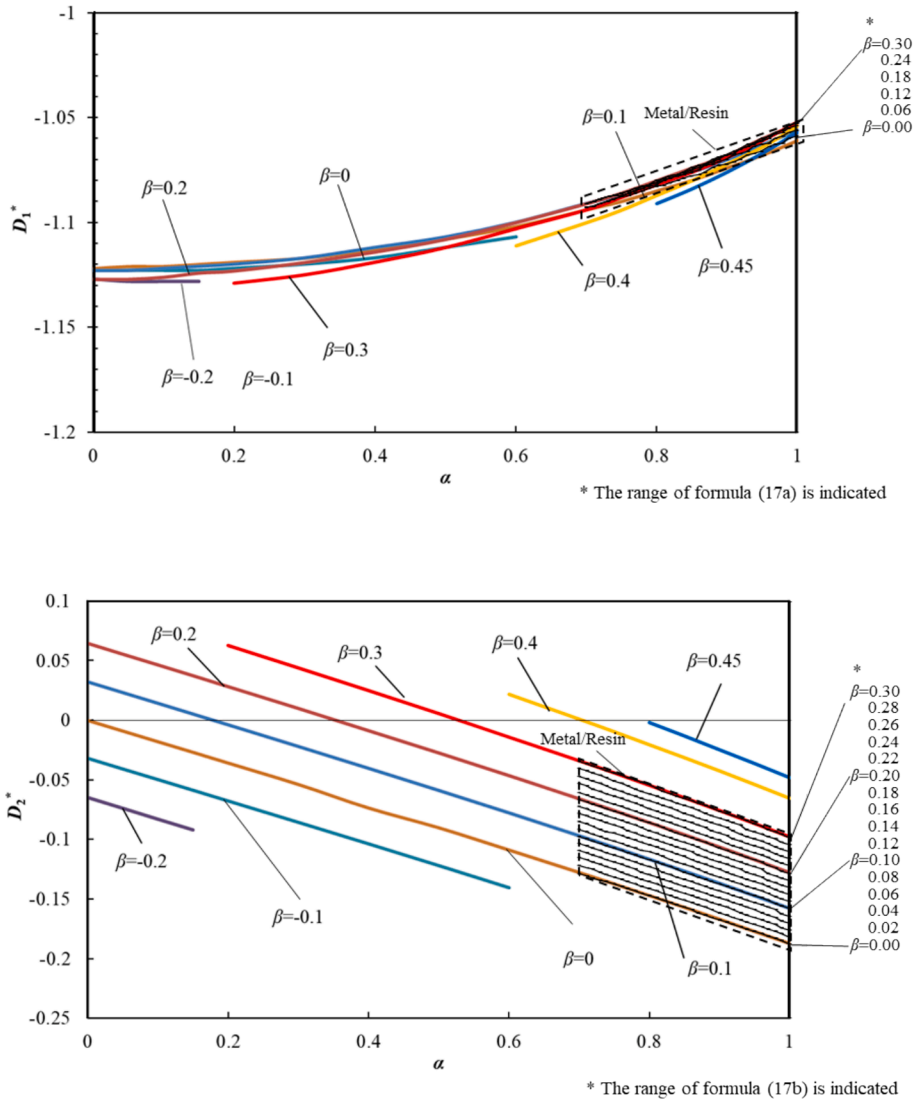

Fig. 16. Values of D_1^*, D_2^* having more than three digits accuracy in Fig. 7(c) when $a/h \le 10^{-2}$, and the error is less than 3 % when $a/h \le 10^{-1}$, $K_1 + iK_2 = (D_1{}^* + iD_2{}^*)\sigma_{y0}\sqrt{\pi a}(1+2i\varepsilon)$, $\sigma_{y0} = \frac{8G_AG_B(\eta_B^*-\eta_A^*)\Delta T}{G_A(\kappa_B-1)-G_B(\kappa_A-1)-2(G_A-G_B)}$, $\eta_m^* = \begin{cases} \eta_m & (plane\ stress) \\ (1+\nu_m)\,\eta_m & (plane\ strain) \end{cases}, (m = \mathrm{A, B})$

are insensitive with less than 3 % error as D_1^*, $D_2^* \approx$ constant when $a/h \le 0.1$. The coefficients D_1^*, D_2^*=constant to three digit when $a/h \le 0.01$.

$$K_1 + iK_2 = \left(D_1^* + iD_2^*\right)\sigma_{y0}\sqrt{\pi a}\left(1+2i\varepsilon\right) \text{ in relation to Fig.7(c)},$$
$$\sigma_{y0} = \frac{8G_AG_B\left(\eta_B^*-\eta_A^*\right)\Delta T}{G_A(\kappa_B-1)-G_B(\kappa_A-1)-2(G_A-G_B)}, \tag{15}$$
$$\eta_m^* = \begin{cases} \eta_m \ \text{(plane stress)} \\ (1+\nu_m)\eta_m \ \text{(plane strain)} \end{cases}, (m = \mathrm{A, B})$$

Fig. 15 shows D_1^*, $D_2^* - h/W$ relation for ABA joints. When the material combinations $\alpha = 0.5, 0.7, 0.8$, β=0.3, $h/W = 0.002 \sim 1.0$. As a result, under the uniform adhesive interface stress distribution the coefficients D_1^*, D_2^* are insensitive to h and determined only by α, β.

Fig. 16 shows the values of the dimensionless coefficients D_1^*, D_2^* in the range $0 \le \alpha \le 1$. From Fig. 16, it is seen that the value of $D_1{}^*$ is in a narrow range of $D_1^* = -1.13 \sim -1.05$, and D_2^* is almost proportional to α for the same β. Accurate values of D_1^*, D_2^* necessary for thermal loading are indicated in Table B3 in Appendix B.

From the discussion above, when $a/h \le 0.1$ and $h/W \le 0.1$ in Fig. 7 (a), the SIF can be provided in the following form under the uniform temperature change ΔT for arbitrary material combination. Note that this expression is valid up to $h/W \le 1$ for adhesive resin.

$$K_1 + iK_2 = (F_1 + iF_2)\sigma_{y0}\sqrt{\pi a}(1+2i\varepsilon),$$
$$F_1 = C_1^*(h/a)^{1-\lambda} + D_1^*,$$
$$F_2 = C_2^*(h/a)^{1-\lambda} + D_2^*$$

$$\sigma_{y0} = \frac{8G_AG_B\left(\eta_B^*-\eta_A^*\right)\Delta T}{G_A(\kappa_B-1)-G_B(\kappa_A-1)-2(G_A-G_B)}, \tag{16}$$
$$\eta_m^* = \begin{cases} \eta_m \ \text{(plane stress)} \\ (1+\nu_m)\eta_m \text{(plane strain)} \end{cases}, (m = \mathrm{A,\ B})$$

The values of C_1^*, C_2^* were indicated in Fig. 12 and Table B1 with the formula for metal/resin in Eq. (14). To express the SIF caused by constant term associated with thermal stress, other coefficients D_1^*, D_2^* are indicated in Fig. 16 and Table B3 for arbitrary material combinations practically used $0 \le \alpha \le 1$. Regarding Metal/resin combination in the range $0.7 \le \alpha$, $0 \le \beta \le 0.3$, the following calculation formula is provided by applying the least square method for readers' convenience.

When $0.7 \le \alpha$, $0 \le \beta \le 0.3$ (Metal/resin combination):

$$D_1^* = -1.0958 - 0.1363\beta + 0.385\beta^2$$
$$+[-0.072658 + 0.38654\beta - 1.3273\beta^2]\alpha$$
$$+[0.10738 - 0.18807\beta + 0.83325\beta^2]\alpha^2 \quad (17a)$$

(less than 0.1 % error).

When $0.7 \le \alpha$, $0 \le \beta \le 0.3$ (Metal/resin combination):

$$D_2^* = -0.005728 + 0.23543\beta + 0.26679\beta^2$$
$$+[-0.15675 + 0.17882\beta - 0.513\beta^2]\alpha$$
$$+[-0.025048 - 0.11952\beta + 0.2619\beta^2]\alpha^2 \quad (17b)$$

(less than 0.2 % error)

6. Critical tensile stress for ABA joint subjected to thermal stress

There are two types of thermosetting adhesives. One is room temperature curing type and the other is heat curing type, and the latter usually has a denser three-dimensional network structure and is said to be stronger than the room temperature curing type. The heat-curing adhesives are widely used after being cured by heating to a temperature higher than room temperature. To evaluate the heat-curing adhesive strength, therefore, it is necessary to consider both the thermal stress generated during heat curing and external loads such as tensile stress. As an example, Fig. 17 shows the critical tensile stress σ_c of at debonding experimentally obtained by the Qian-Akisanya [23]. This experiment uses ABA joints composed of A = aluminum, B = epoxy F922 and thermally stressed when the width $W = 30$ mm and the thickness $t = 10$mm. In Fig. 17, the symbol ◇ denotes the critical tensile stress when aluminum plates were bonded with epoxy resin at a temperature of $T_0 = 120^\circ$C, the temperature was maintained for 8 h to harden the adhesive, and then the temperature was cooled to room temperature $T_0 = 20^\circ$C. In other words, the symbol ◇ denotes the critical stress $\sigma_c = \sigma_c(\Delta T)$ for the residual stress due to the temperature difference of $\Delta T = T - T_0 = -100^\circ$C. Similarly, the symbol ■ denotes the critical stress when aluminum plates were bonded with epoxy resin at a temperature of $T_0 = 160^\circ$C, the temperature was maintained for 6 h to harden the adhesive, and then the temperature was cooled to room temperature $T_0 = 20^\circ$C. In other words, the symbol ■ denotes the critical stress σ_c for the residual stress due to the temperature difference $\Delta T = T - T_0 = -140^\circ$C. The dotted lines in Fig. 17 can be obtained by applying the SIF solution in this paper and the detail will be discussed later.

Table 4
Elastic and thermal properties of the epoxy resins and the aluminum substrates in ABA joint in Fig. 17∼Fig. 20.

Material combination	Young's modulus, E [GPa]	Poisson's ratio ν	Thermal expansion [K^{-1}]	α	β	λ
Aluminum alloy	70	0.35	2.1×10^{-5}	0.894	0.171	0.718
F922 epoxy	3.8	0.38	5.8×10^{-5}			

Table 4 shows elastic and thermal properties of the epoxy resins and the aluminum substrates in this ABA joint necessary to calculate the SIF of the fictitious crack [23]. By substituting $\alpha = 0.894$ and $\beta = 0.171$ in Table 4 into Eq. (14) and Eq. (17), which is useful for metal/resin combination, the values $C_1^* = 0.5429$, $C_2^* = -0.1098$, $D_1^* = -1.069$, $D_2^* = -0.1142$ can be obtained. By using these values with Eq. (16), the SIF $K_1^{\Delta T}$ due to temperature change ΔT can be determined. Similarly, by using the values of $C_1^* = 0.5429$, $C_2^* = -0.1098$ and the critical stress σ_c experimentally obtained in Fig. 17(b), $K_1^{\sigma_c}$ due to $\sigma_{y0} = \sigma_c$ can be determined from Eq. (12).

Fig. 18 shows the critical value of SIF, K_{1C} (fracture toughness) determined from a fictitious edge interface crack length $a = 10^{-4}$mm and the critical tensile stress σ_c experimentally determined. As shown in Fig. 18(b), the adhesive strength can be expressed as $K_{1C} = K_{1C}^{\Delta T+\sigma_c} = K_1^{\Delta T} + K_1^{\sigma_c} =$ constant $= 6.34\text{MPa}\sqrt{\text{mm}}$ when a fictitious crack length $a = 10^{-4}$mm independent of temperature change ΔT.

$$K_{1C} = K_{1C}^{\Delta T+\sigma_c} = K_1^{\Delta T} + K_1^{\sigma_c} = \text{constant}$$
$$= 6.34\text{MPa}\sqrt{\text{mm}}\ (\text{when } a = 10^{-4}\text{mm}) \quad (18)$$

As shown in Eq. (18), the adhesive strength can be expressed as K_{1C} = constant, which is much more convenient than σ_c varying depending on ΔT and h. Fig. 18(c) shows the SIF ratio K_{2C}/K_{1C} = constant like K_{1C}

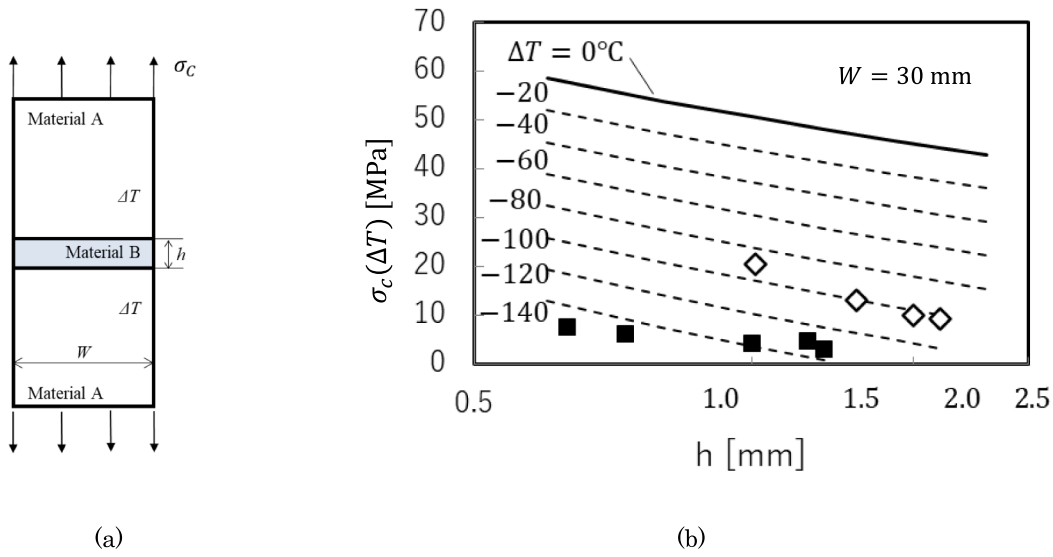

Fig. 17. Critical tensile stress at debonding of ABA joints thermally stressed (A = aluminum, B = epoxy F922, α=0.894, $\beta = 0.171$). The experiment was conducted for the width $W = 30$ mm and the thickness $t = 10$ mm. Here, ΔT ($=T - T_0$) is a uniform temperature change from the curing temperature T_0 to the room temperature T ($T < T_0$). The marks ◇ and ■ are the experimental data obtainded by Qian-Akisanya [23] for $\Delta T = -100^\circ$C and -140°C, respectively. The solid and dashed lines show the critical tensile stress calculated from K_{1c} = constant using the fictitious crack method when ΔT is changed.

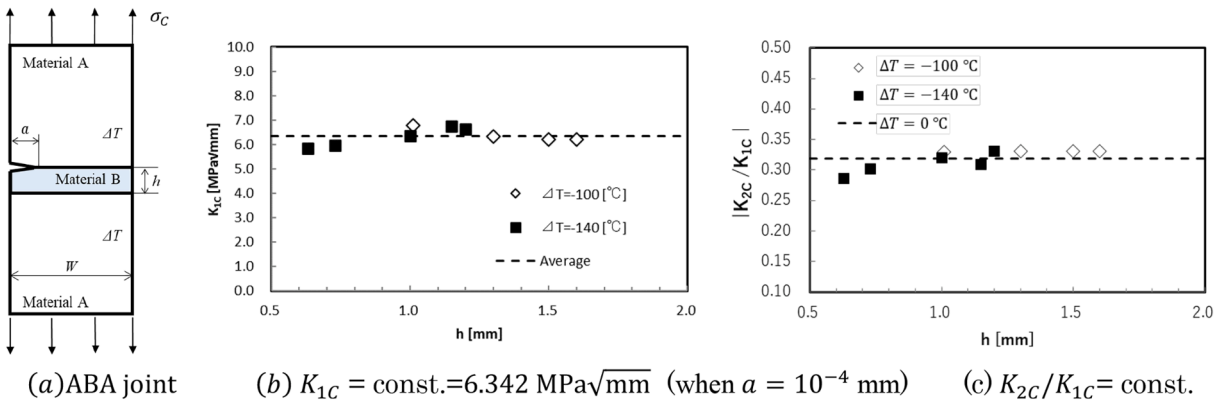

Fig. 18. ABA joint strength expressed as SIFK_{1C} = const when a fictitious crack length $a = 10^{-4}$ mm is assumed for A = alminium, B = epoxy (F922), α = 0.894, β = 0.171.

= constant. If the fictitious crack length "a" differs, the critical value will be different, but it will still be a constant value. In other words, the critical value varies depending on the fictitious crack length "a", but the constant K_{1C} can be used to express the strength of this ABA joint Similar to Fig. 18, Qian-Akisanya [23] showed that the adhesive strength of the ABA joint can be expressed as the ISSF = constant (see Fig.A2 in Appendix A). Those analyses assume a constant linear expansion coefficient and a constant Young's modulus of thermosetting epoxy adhesives independent of temperature [22,23].

As discussed above, K_{1C}=constant in Fig. 18 can be obtained by applying the fictitious crack method by calculating the SIF. They can be provided from coefficients C_1^*, C_2^*, D_1^*, D_2^* in Eqs. (14), (17) without performing extra FEM calculations. The ABA joint tensile strength $\sigma_c(\Delta T)$ subjected to temperature change ΔT can be evaluated by assuming a fictitious edge interface crack in ABA joints. This is because the SIF of the crack is totally dominated by the ISSF at the crack-free interface end. The usefulness of the SIF solution can be expressed as shown in Eq. (19), which represents the critical tensile strength $\sigma_c(\Delta T)$.

$$\sigma_c(\Delta T) = (K_{1C}^{\Delta T+\sigma_c} - K_1^{\Delta T})/K_1^{\sigma_c}|_{\sigma_c(\Delta T)=1},$$

$$K_{1C}^{\Delta T+\sigma_c} = K_1^{\Delta T} + K_1^{\sigma_c} = 6.34\text{MPa}\sqrt{\text{mm}} \text{ (when } a = 10^{-4}\text{mm)},$$

$$K_1^{\Delta T} = \left[\left\{C_1^*(h/a)^{1-\lambda} + D_1^*\right\} - 2\varepsilon\left\{C_2^*(h/a)^{1-\lambda} + D_2^*\right\}\right]\sigma_{y0}\sqrt{\pi a},$$

$$K_1^{\sigma_c}|_{\sigma_c(\Delta T)=1} = \left(C_1^* - 2\varepsilon C_2^*\right)(h/a)^{1-\lambda}\sqrt{\pi a}$$

$$\sigma_{y0} = \frac{8G_AG_A\left(\eta_B^* - \eta_A^*\right)\Delta T}{G_A(\kappa_B - 1) - G_B(\kappa_A - 1) - 2(G_A - G_B)} \tag{19}$$

As well as the experimental results, Fig. 17 also shows the results of Eq. (19) as the dotted line by varying the temperature change ΔT. The results of $\sigma_c(\Delta T)$ for $\Delta T = -100^\circ$C, $\Delta T = -140^\circ$C agree with the experimental results within about ±4 MPa. With decreasing the temperature difference ΔT, the critical stress $\sigma_c(\Delta T)$ increases significantly. Fig. 18 and the following Fig. 19, Fig. 20 are based on $K_{1C}^{\Delta T+\sigma_c}$=$K_1^{\Delta T}$ + $K_1^{\sigma_c}$=6.34MPa$\sqrt{\text{mm}}$ (when $a = 10^{-4}$ mm) in Eq. (19).

To clarify the amount of the thermal SIF $K_1^{\Delta T}$ in the critical SIF $K_{1C}^{\Delta T+\sigma_c} = K_1^{\Delta T} + K_1^{\sigma_c}$ at debonding, Fig. 19 illustrates the variation of $K_1^{\Delta T}$ in Eq. (19) when $\Delta T = -20, -40, -60, \cdots, -140^\circ$C. With increasing ΔT, the amount of $K_1^{\Delta T}$ increases, although a certain amount of ΔT necessary for cure of thermosetting resin.

Under constant ΔT, the amount of $K_1^{\Delta T}$ decreases with deceasing the adhesive thickness h. For example, when $\Delta T = -140^\circ$C, it is seen that $K_1^{\Delta T} \cong K_{1C}^{\Delta T+\sigma_c}$ at $h = 1.3$ mm. Therefore, the ABA joint may be deboned only due to thermal stress at $\Delta T = -140^\circ$C and $h = 1.3$ mm. With decreasing ΔT, $K_1^{\Delta T}$ becomes insensitive to the adhesive layer thickness

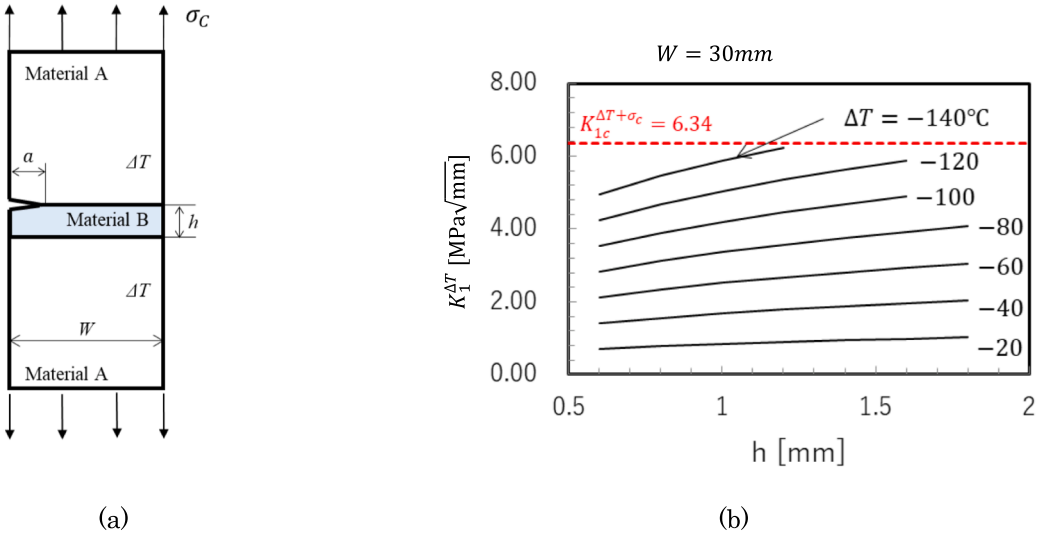

Fig. 19. Effect of thermal SIF $K_1^{\Delta T}$ due to temperature change ΔT on the critical SIF $K_{1C}^{\Delta T+\sigma_c} = K_1^{\Delta T} + K_1^{\sigma_c}$ when a fictitious crack length $a = 10^{-4}$ mm assumed for alminium/epoxy (F922), W = 30 mm, α=0.894, β = 0.171.

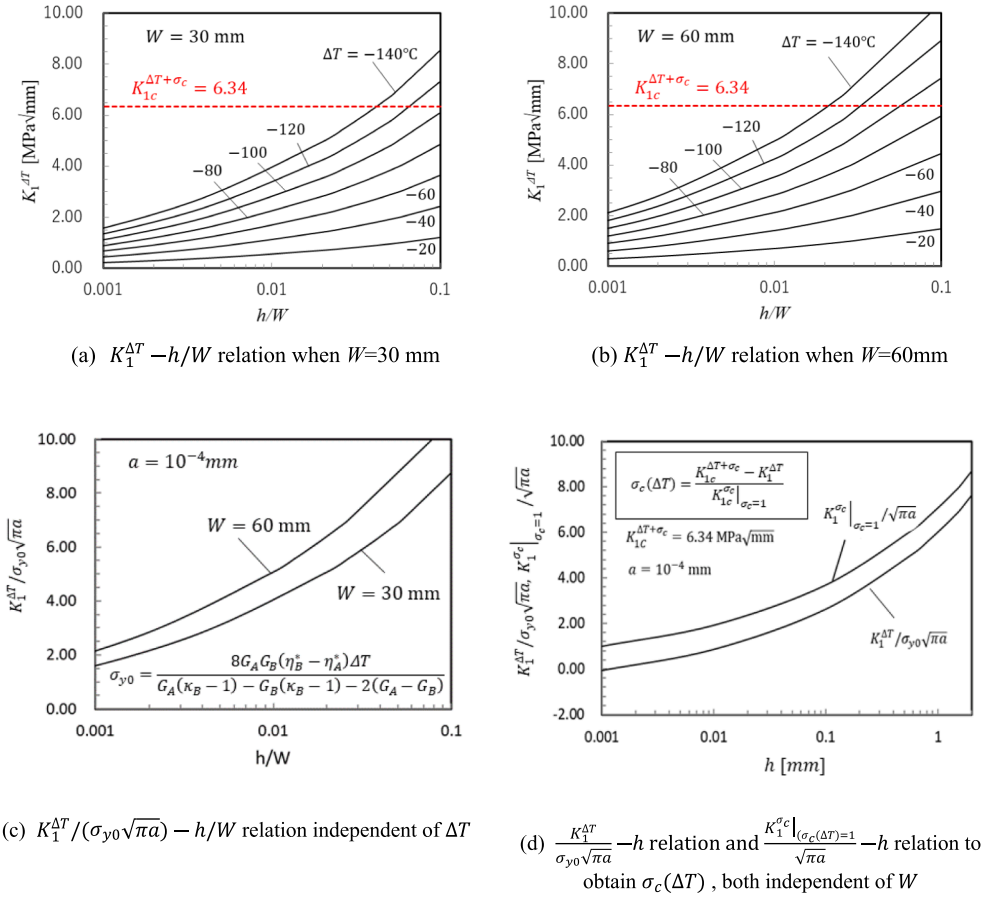

(a) $K_1^{\Delta T} - h/W$ relation when W=30 mm

(b) $K_1^{\Delta T} - h/W$ relation when W=60mm

(c) $K_1^{\Delta T}/(\sigma_{y0}\sqrt{\pi a}) - h/W$ relation independent of ΔT

(d) $\frac{K_1^{\Delta T}}{\sigma_{y0}\sqrt{\pi a}} - h$ relation and $\frac{K_1^{\sigma_c}|_{(\sigma_c(\Delta T)=1}}{\sqrt{\pi a}} - h$ relation to obtain $\sigma_c(\Delta T)$, both independent of W

Fig. 20. Thermal SIF $K_1^{\Delta T}$ due to temperature change ΔT by varying the adhesive area W and the adhesive layer thickness h for alminium/epoxy (F922) ABA joint.

h.

Qian-Akisanya used the ABA joint specimen whose width$W = 30$ mm [23], but $K_{1C}^{\Delta T+\sigma_c} = K_1^{\Delta T} + K_1^{\sigma_c} = 6.34\text{MPa}\sqrt{\text{mm}}$ can be applied to other specimen width W. Fig. 20 illustrates $K_1^{\Delta T} - h/W$ relation in the ABA joint having a similar shape when $W = 30$ mm and $W = 60$ mm. Fig. 20 (a)~(d) can be provided from the critical SIF $K_{1C}^{\Delta T+\sigma_c} = K_1^{\Delta T} + K_1^{\sigma_c} = 6.34\text{MPa}\sqrt{\text{mm}}$. Fig. 20 (a), (b) show $K_1^{\Delta T} - h/W$ relation (a) when$W =$ 30 mm, and (b) when $W = 60$ mm. From the comparison between Fig. 20 (a) and (b), to obtain the same value of $K_1^{\Delta T}$, the relative adhesive thickness h/W is smaller when $W = 60$ mm. For example, when $W = 30$ mm and $\Delta T = -140^{\circ}$C, $K_1^{\Delta T} \cong K_{1C}^{\Delta T+\sigma_c}$ at $h/W = 0.04$ but when $W = 60$ mm and $\Delta T = -140^{\circ}$C, $K_1^{\Delta T} \cong K_{1C}^{\Delta T+\sigma_c}$ at $h/W = 0.02$.

Fig. 20(c) shows the normalized SIF $K_1^{\Delta T}/(\sigma_{y0}\sqrt{\pi a}) - h/W$ relation by using σ_{y0}. As shown in Fig. 20(c), although $K_1^{\Delta T}$ varies depending on ΔT as can be expressed $K_1^{\Delta T} = K_1^{\Delta T}(\Delta T)$ in Fig. 20(a), (b), $K_1^{\Delta T}/(\sigma_{y0}\sqrt{\pi a})$ can be expressed as a single curve independent of ΔT. As shown in Fig. 20(c), with increasing the plate width W, the value of $K_1^{\Delta T}/\sigma_{y0}\sqrt{\pi a}$ increases. In this way, the SIF $K_1^{\Delta T}$ due to thermal stress cannot be directly applied to specimens with similar dimensions h/W, and care must be taken.

Fig. 20(d) shows $K_1^{\Delta T}/(\sigma_{y0}\sqrt{\pi a}) - h$ relation by changing the horizontal axis to h in Fig. 20(c). By setting h to the horizontal axis, $K_1^{\Delta T}/(\sigma_{y0}\sqrt{\pi a})$ becomes independent of W. Fig. 20(d) also shows the value of $K_1^{\sigma_c}|_{\sigma_c(\Delta T)=1}/\sqrt{\pi a}$, which is necessary for calculating $\sigma_c^{\Delta T}$. From Fig. 20 with $K_{1C}^{\Delta T+\sigma_c} = 6.34\text{MPa}\sqrt{\text{mm}}$ (when $a = 10^{-4}$mm), the critical stress $\sigma_c(\Delta T)$ can be calculated for any h, ΔT by substituting $K_1^{\Delta T}, K_1^{\sigma_c}|_{\sigma_c(\Delta T)=1}$ in Fig. 20 (d) into Eq. (19).

In this paper, a useful thermal SIF solution was proposed by superposing the SIF under tensile stress and the SIF under uniform interface stress associated with thermal load. This general SIF solution under arbitrary material combination can be applied for predicting the tensile strength σ_c and critical temperature change ΔT without performing extra FEM calculations. The usefulness of the solution was confirmed through Aluminum/Epoxy butt joint strength experimentally obtained. In other words, the tensile strength σ_c can be predicted for various temperature change ΔT and for various adhesive layer thickness h fromK_{1C} = constant of a fictitious interface crack.

7. Conclusions

The ABA joint specimens usually called butt joints are essential for evaluating the thermal adhesive strength as well as the tensile adhesive strength. The adhesive strength can be discussed from the stress intensity factor (SIF) of a fictitious edge interface crack assumed at the interface end. This is because the SIF of the crack is totally dominated by the ISSF at the edge of the crack-free interface. In this paper, therefore, the SIF of an edge interface crack in the ABA joints was investigated by varying crack length and adhesive layer thicknesses under arbitrary material combinations. The solution presented in this paper is especially useful for heat-curing adhesives because they are widely used after being cured by heating to a temperature higher than room temperature. The conclusions can be summarized in the following way.

(1) A useful thermal SIF solution for ABA joint was proposed by superposing the SIF under tensile stress σ_y and the SIF under uniform interface stress associated with thermal load ΔT. This general SIF solution provided under arbitrary material combination can be applied for predicting the tensile strength σ_c and

critical temperature change ΔT without performing new FEM calculations.

(2) When $a/h \leq 0.1$ and $h/W \leq 0.1$ in Fig. 1(a), the thermal SIF solution can be provided in the following form under a uniform temperature change ΔT for arbitrary material combination. Also, without using D_1^*, D_2^*, this expression can be used as the SIF solution under tension as shown in Fig. 1(b). The SIF for interface edge crack in ABA joints has less than 3 % error when $a/h \leq 0.1$ and three-digit accuracy when $a/h \leq 0.01$.

$$K_1 + iK_2 = (F_1 + iF_2)\sigma_{y0}\sqrt{\pi a}(1 + 2i\varepsilon),\ F_1 = C_1^*(h/a)^{1-\lambda} + D_1^*,$$
$$F_2 = C_2^*(h/a)^{1-\lambda} + D_2^*,$$

$$\sigma_{y0} = \frac{8G_AG_B(\eta_B^* - \eta_A^*)\Delta T}{G_A(\kappa_B - 1) - G_B(\kappa_A - 1) - 2(G_A - G_B)},$$
$$\eta_m^* = \begin{cases} \eta_m\ (\text{plane stress}) \\ (1+\nu_m)\eta_m (\text{plane strain}) \end{cases} (m = \text{A, B})$$

The values of C_1^*, C_2^* are indicated in Fig. 12 and Table B1 and the values D_1^*, D_2^* are indicated in Fig. 16 and Table B3 for arbitrary material combinations practically used $0 \leqq \alpha \leqq 1$. Furthermore, the approximate formulas for calculating C_1^*, C_2^* and D_1^*, D_2^* were presented in Eqs. (14) and (17) for metal/resin combination in the range $\alpha \geq 0.7$ and $0 \leq \beta \leq 0.3$.

(3) The usefulness of the SIF solution was confirmed for Aluminum/Epoxy ABA joints subjected to both thermal stress due to ΔT and mechanical stress σ_y. From the critical tensile stress $\sigma_y = \sigma_c(\Delta T)$ experimentally obtained, the SIF of a fictitious crack was calculated as $K_1^{\sigma_c}$. Also, from the temperature change ΔT, the SIF was calculated as $K_1^{\Delta T}$. Then, the critical SIF was obtained as $K_1^{\Delta T+\sigma_c} = K_1^{\Delta T} + K_1^{\sigma_c}$ by using the present SIF solution. Without performing extra FEM analysis, the adhesive strength was expressed as $K_{1C} =$ constant for various temperature change ΔT and for various adhesive bondline thickness h (see Fig. 18). This is useful for predicting the adhesive strength $\sigma_c(\Delta T)$ for various adhesive geometries. The results showed that with increasing ΔT, the amount of $K_1^{\Delta T}$ increases, although a certain amount of ΔT necessary for cure of heat-curing adhesives.

CRediT authorship contribution statement

Kazuhiro Oda: Writing – original draft, Validation, Project administration, Methodology, Investigation, Funding acquisition, Conceptualization. **Hiroki Oda:** Validation, Formal analysis. **Yasushi Takase:** Visualization, Validation, Formal analysis. **Nao-Aki Noda:** Writing – review & editing, Methodology.

Declaration of competing interest

The authors declare the following financial interests/personal relationships which may be considered as potential competing interests: [Kazuhiro Oda reports financial support was provided by Japan Society for the Promotion of Science. If there are other authors, they declare that they have no known competing financial interests or personal relationships that could have appeared to influence the work reported in this paper].

Data availability

Data will be made available on request.

Acknowledgments

This work was partially supported by Japan Society for the Promotion of Science, JSPS KAKENHI Grant Number JP 21 K03818, Japan.

Appendix A. Normalized ISSF of a semi-infinite ABA joint in Fig. 4(b) under tension and thermal loading

Table A1 and Fig. A1 show the normalized ISSF $F_\sigma^* = K_\sigma/\sigma h^{1-\lambda}$ of ABA joint in Fig. 4(b) under arbitrary material combinations. Those results are useful in the range $h/W \leq 0.01$ in Fig. 4(a) and can be used within 10 % error for $h/W \leq 0.1$ in Fig. 4(a). The accurate results can be obtained by the interpolation in the range for $0.01 \leq h/W \leq 1.0$ under arbitrary material combination.

Table A1
Normalized ISSF $F_\sigma^* = K_\sigma/\sigma h^{1-\lambda}$ of ABA joint in Fig. 4(b) which is useful for $h/W \leq 0.01$ in Fig. 4(a).

α	$\beta = -0.4$	$\beta = -0.3$	$\beta = -0.2$	$\beta = -0.1$	$\beta = 0$	$\beta = 0.1$	$\beta = 0.2$	$\beta = 0.3$	$\beta = 0.4$
−1.0	1.134	1.209	1.315	1.404	1.498				
−0.9	1.066	1.148	1.252	1.347	1.424				
−0.8	1.000	1.082	1.191	1.289	1.352				
−0.7	0.904	1.032	1.134	1.223	1.288				
−0.6		0.990	1.075	1.156	1.227	1.420			
−0.5		0.946	1.028	1.119	1.185	1.360			
−0.4		0.901	1.000	1.092	1.166	1.320			
−0.3		0.812	0.940	1.057	1.142	1.280			
−0.2		0.680	0.837	1.000	1.113	1.250	1.500		
−0.1			0.710	0.916	1.061	1.230	1.460		
0			0.585	0.799	1.000	1.195	1.430		
0.1			0.460	0.654	0.873	1.124	1.380		
0.2			0.353	0.550	0.758	1.000	1.314	1.918	
0.3				0.456	0.643	0.858	1.181	1.769	
0.4				0.384	0.558	0.740	1.000	1.572	
0.5				0.326	0.476	0.630	0.813	0.293	
0.6				0.3257	0.405	0.546	0.686	1.000	
0.7					0.340	0.470	0.588	0.794	1.730
0.8					0.290	0.403	0.506	0.634	1.000
0.9					0.223	0.333	0.430	0.543	0.746
1.0					0.169	0.265	0.358	0.456	0.495

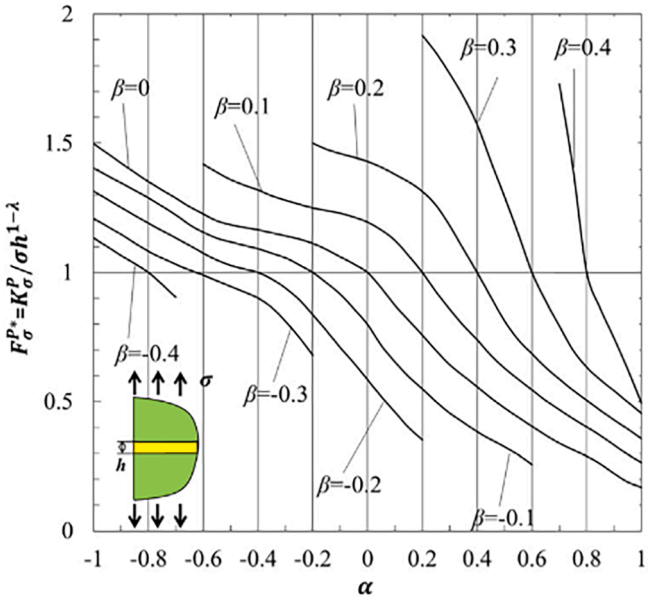

Fig. A1. Normalized ISSF of ABA joint in Fig. 4(b) which is useful for in Fig. 4(a).

Like $K_{1C} = 6.34\text{MPa}\sqrt{\text{mm}}$ of the fictitious crack length (when $a = 10^{-4}$mm) in Fig. 18, Fig. A2 shows the ABA joint strength expressed as ISSF $K_{\sigma C}$ = const. As shown in Fig. A2, without using the fictitious crack, the adhesive strength can be expressed as a sum of the ISSF due to tensile loading and the ISSF due to thermal loading. The result in Fig. A2 is in good agreement with the one of Qian-Akisanya [23]. It may be concluded that Eqs. (5), (6) with Table A1 and Fig. A1 are useful for adhesive strength. Both the ISSF method and the fictitious crack method express the adhesive strength. The ISSF method simply uses only K_σ. Instead, the fictitious crack method may have an advantage indicating the effect of shear stress τ_{xy} on the delamination stress σ_y from the stress ratio K_2/K_1 by using two parameters K_1, K_2.

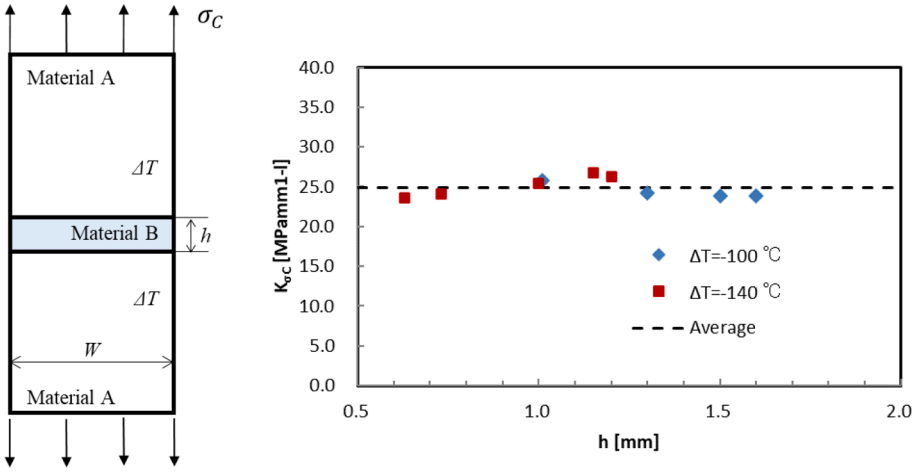

Fig. A2. ABA joint strength expressed as ISSF = const for alminium/epoxy (F922), ,

Appendix B. SIF of an edge crack in AB joint corresponding to $h/W \geq 1.0$ in ABA joint

Table B1 shows the coefficients $C_1^* = F_1/(h/a)^{1-\lambda}$ and $C_2^* = F_2/(h/a)^{1-\lambda}$ (solid lines in Fig. 12) of the ABA joint in Fig. 7(b) for arbitrary material combinations. These results are useful in the range $h/W \leq 0.01$ in Fig. 7(b), and within 10 % error for $h/W \leq 0.1$ in Fig. 7(b). Table B2 also shows the coefficients $C_1 = F_1/(W/a)^{1-\lambda}$ and $C_2 = F_2/(W/a)^{1-\lambda}$ (dashed line in Fig. 12) of the AB joint in Fig. 7(b) for arbitrary material combinations. For any combination of materials, accurate results can be obtained by interpolation in the range $0.01 \leq h/W \leq 1.0$.

Table B3 shows the coefficients D_1^* and D_2^* (Fig. 16) of the ABA joint in Fig. 7(c) for arbitrary material combinations. These results are useful in the range $a/h \leq 0.01$ in Fig. 7(c) and are independent of h/W.

Table B1
Values of C_1^* and C_2^* having more than three digits accuracy in the range $a/h \leq 0.1$ and $h/W \leq 0.1$ in Fig. 7 (b) subjected to tension σ_{y0} [$K_1 + iK_2 = (F_1 + iF_2)\sigma_{y0}\sqrt{\pi a}(1 + 2i\varepsilon)$, $F_1 = C_1^*(h/a)^{1-\lambda}$, $F_2 = C_2^*(h/a)^{1-\lambda}$]

Values of C_1^*

α	$\beta = -0.2$	$\beta = -0.1$	$\beta = 0$	$\beta = 0.1$	$\beta = 0.2$	$\beta = 0.3$	$\beta = 0.4$	$\beta = 0.45$
0.00	0.6266	0.8831	1.1215	1.3249	1.4828			
0.05	0.5749	0.8201	1.0630	1.2869	1.4732			
0.10	0.5292	0.7521	1.0004	1.2396	1.4571			
0.15	0.4884	0.7054	0.9368	1.1832	1.4335			
0.20		0.6552	0.8746	1.1197	1.3955	1.6009		
0.30		0.5817	0.7610	0.9842	1.2742	1.7047		
0.40		0.4958	0.6655	0.8568	1.1141	1.5988		
0.50		0.4320	0.5855	0.7486	0.9568	1.3551		
0.60		0.3610	0.5168	0.6595	0.8256	1.1038	1.7168	
0.70			0.4542	0.5849	0.7213	0.9123	1.3120	
0.75			0.4235	0.5514	0.6774	0.8383	1.0871	
0.80			0.3918	0.5195	0.6379	0.7759	0.9413	1.4672
0.85			0.3578	0.4885	0.6021	0.7226	0.8385	1.0753
0.90			0.3176	0.4571	0.5691	0.6770	0.7620	0.8948
0.95			0.2616	0.4228	0.5384	0.6384	0.6667	0.7370
1.00			0.1569	0.3678	0.4891	0.5785	1.7168	1.4672

Values of C_2^*

α	$\beta = -0.2$	$\beta = -0.1$	$\beta = 0$	$\beta = 0.1$	$\beta = 0.2$	$\beta = 0.3$	$\beta = 0.4$	$\beta = 0.45$
0.00	−0.1219	−0.0872	0.0000	0.1306	0.2883			
0.05	−0.1212	−0.0987	−0.0253	0.0932	0.2594			
0.10	−0.1192	−0.1056	−0.0472	0.0647	0.2271			
0.15	−0.1165	−0.1121	−0.0655	0.0331	0.1919			
0.20		−0.1153	−0.0800	0.0041	0.1539	0.3513		
0.30		−0.1114	−0.0996	−0.0429	0.0758	0.3153		
0.40		−0.1152	−0.1089	−0.0746	0.0086	0.2092		
0.50		−0.1103	−0.1142	−0.0939	−0.0394	0.0961		
0.60		−0.0984	−0.1144	−0.1050	−0.0700	0.0138		
0.70			−0.1110	−0.1104	−0.0888	−0.0363	0.1575	
0.75			−0.1080	−0.1116	−0.0952	−0.0529	0.0700	
0.80			−0.1039	−0.1117	−0.1000	−0.0658	0.0204	
0.85			−0.0982	−0.1109	−0.1035	−0.0758	−0.0114	0.0925
0.90			−0.0901	−0.1090	−0.1061	−0.0837	−0.0333	0.0246
0.95			−0.0764	−0.1054	−0.1076	−0.0901	−0.0493	−0.0099
1.00			−0.0469	−0.0947	−0.1028	−0.0893	−0.0554	−0.0257

Table B2
Values of C_1 and C_2 having more than three digits accuracy in the range $a/W < 10^{-3}, h/W \geq 1.0$ in Fig. 7 (b) subjected to tension σ_{y0} [$K_1 + iK_2 = (F_1 + iF_2)\sigma_{y0}\sqrt{\pi a}(1 + 2i\varepsilon)$, $F_1 = C_1(W/a)^{1-\lambda}$, $F_2 = C_2(W/a)^{1-\lambda}$].

Values of C_1

α	$\beta = -0.2$	$\beta = -0.1$	$\beta = 0$	$\beta = 0.1$	$\beta = 0.2$	$\beta = 0.3$	$\beta = 0.4$	$\beta = 0.45$
0.00	1.071	1.103	1.122	1.103	1,071			
0.05	1.009	1.074	1.114	1.132	1.120			
0.10	0.952	1.034	1.093	1.142	1.166			
0.15	0.881	0.991	1.063	1.138	1.201			
0.20		0.947	1.024	1.119	1.221	1.570		
0.30		0.863	0.938	1.046	1.202	1.530		
0.40		0.786	0.852	0.952	1.113	1.449		
0.50		0.711	0.773	0.857	0.991	1.306		
0.60		0.645	0.702	0.771	0.872	1.103	2.485	
0.70			0.637	0.694	0.769	0.920	1.593	
0.75			0.606	0.659	0.723	0.843	1.297	
0.80			0.576	0.627	0.679	0.777	1.086	1.868
0.85			0.546	0.595	0.640	0.719	0.928	1.408
0.90			0.533	0.565	0.603	0.666	0.815	1.075
0.95			0.519	0.537	0.568	0.619	0.727	0.869
1.00			0.510	0.500	0.535	0.559	0.644	0.790

Values of C_2

α	β = 0.2	β= 0.1	β = 0	β= 0.1	β= 0.2	β= 0.3	β= 0.4	β= 0.45
0.00	−0.210	−0.113	0.000	0.111	0.209			

(continued on next page)

Table B2 (*continued*)

Values of C_2								
α	β = 0.2	β= 0.1	β = 0	β= 0.1	β= 0.2	β= 0.3	β= 0.4	β= 0.45
0.05	−0.212	−0.129	−0.027	0.085	0.198			
0.10	−0.214	−0.145	−0.052	0.059	0.181			
0.15	−0.209	−0.157	−0.074	0.031	0.159			
0.20		−0.167	−0.093	0.004	0.133	0.349		
0.30		−0.178	−0.123	−0.046	0.070	0.273		
0.40		−0.183	−0.141	−0.083	0.008	0.181		
0.50		−0.181	−0.151	−0.108	−0.041	0.089		
0.60		−0.177	−0.155	−0.123	−0.075	0.013	0.195	
0.70			−0.155	−0.132	−0.095	−0.037	0.130	
0.75			−0.153	−0.134	−0.102	−0.054	0.065	
0.80			−0.151	−0.135	−0.107	−0.067	0.020	0.134
0.85			−0.147	−0.136	−0.111	−0.076	−0.012	0.079
0.90			−0.145	−0.135	−0.113	−0.083	−0.033	0.024
0.95			−0.142	−0.134	−0.114	−0.088	−0.048	−0.011
1.00			−0.139	−0.129	−0.101	−0.087	−0.061	−0.026

Table B3

Values of D_1^*, D_2^* having more than three digits accuracy in the range $a/W \leq 10^{-3}$ subjected to ΔT and σ_{y0} as shown in Fig. 7(c) [$K_1 + iK_2 = (D_1^* + iD_2^*)\sigma_{y0}\sqrt{\pi a}(1 + 2i\varepsilon)$].

Values of D_1*								
α	β = -0.2	β = -0.1	β = 0	β = 0.1	β = 0.2	β = 0.3	β = 0.4	β = 0.45
0.00	−1.127	−1.123	−1.122	−1.123	−1.127			
0.05	−1.128	−1.123	−1.121	−1.123	−1.127			
0.10	−1.128	−1.123	−1.121	−1.122	−1.126			
0.15	−1.128	−1.123	−1.120	−1.121	−1.124			
0.20		−1.122	−1.119	−1.120	−1.123	−1.129		
0.30		−1.120	−1.117	−1.117	−1.119	−1.125		
0.40		−1.117	−1.113	−1.112	−1.114	−1.119		
0.50		−1.112	−1.108	−1.107	−1.108	−1.112		
0.60		−1.107	−1.102	−1.100	−1.100	−1.103	−1.111	
0.70			−1.094	−1.091	−1.091	−1.094	−1.100	
0.75			−1.090	−1.087	−1.086	−1.088	−1.094	
0.80			−1.085	−1.081	−1.080	−1.082	−1.087	−1.091
0.85			−1.080	−1.076	−1.074	−1.076	−1.080	−1.084
0.90			−1.074	−1.070	−1.068	−1.069	−1.072	−1.076
0.95			−1.068	−1.063	−1.060	−1.061	−1.064	−1.067
1.00			−1.061	−1.056	−1.053	−1.052	−1.054	−1.057
Values of D_2*								
α	β = -0.2	β = -0.1	β = 0	β = 0.1	β = 0.2	β = 0.3	β = 0.4	β = 0.45
0.00	−0.0647	−0.0318	0.0000	0.0318	0.0647			
0.05	−0.0737	−0.0408	−0.0089	0.0229	0.0556			
0.10	−0.0828	−0.0497	−0.0179	0.0139	0.0466			
0.15	−0.0918	−0.0587	−0.0268	0.0049	0.0375			
0.20		−0.0677	−0.0358	−0.0041	0.0283	0.0629		
0.30		−0.0857	−0.0538	−0.0222	0.0100	0.0441		
0.40		−0.1038	−0.0736	−0.0405	−0.0087	0.0251		
0.50		−0.1221	−0.0902	−0.0590	−0.0274	0.0058		
0.60		−0.1407	−0.1089	−0.0778	−0.0465	−0.0140	0.0217	
0.70			−0.1278	−0.0970	−0.0660	−0.0338	0.0009	
0.75			−0.1374	−0.1067	−0.0759	−0.0440	−0.0097	
0.80			−0.1472	−0.1166	−0.0860	−0.0544	−0.0206	−0.0020
0.85			−0.1571	−0.1266	−0.0962	−0.0649	−0.0314	−0.0132
0.90			−0.1671	−0.1368	−0.1066	−0.0756	−0.0425	−0.0248
0.95			−0.1774	−0.1472	−0.1172	−0.0865	−0.0539	−0.0363
1.00			−0.1875	−0.1578	−0.1281	−0.0977	−0.0655	−0.0482

References

[1] T.A. Barnes, I.R. Pashby, Joining techniques for aluminium spaceframes used in automobiles: Part II -adhesive bonding and mechanical fasteners, J Mater Process Technol 99 (1–3) (2000) 72–79.

[2] D.E. Packham, Adhesive technology and sustainability, Int J Adhesion Adhes. 29 (2009) 248–252.

[3] M. Goede, M. Stehlin, L. Rafflenbeul, G. Kopp, E. Beeh, Super Light Car – lightweight construction thanks to a multi-material design and function integration, Eur Transp Res Rev 1 (2009) 5–10.

[4] S. Kleemann, T. Fröhlich, E. Türck, T. Vietor, T.,, A methodological approach towards multi-material design of automotive components, Procedia CIRP 60 (2017) 68–73.
[5] B. Watson, Y. Nandwani, M.J. Worswick, D.S. Cronin, Metallic multi-material adhesive joint testing and modeling for vehicle lightweighting, Int J Adhesion Adhes 95 (2019) 102421.
[6] D. Blanco, E.M. Rubio, M.M. Marín, J.P. Davim, Advanced materials and multi-materials applied in aeronautical and automotive fields: a systematic review approach, Procedia CIRP 99 (2021) 196–201.
[7] D.B. Bogy, Edge bonded dissimilar orthogonal elastic wedges under normal and shear loadings, J. Appl. Mech. 35 (1968) 460–466.
[8] D.B. Bogy, K.C. Wang, Stress singularities at interface corners in bonded dissimilar isotropic elastic materials, J. Solids Struct. 7 (1971) 993–1005.
[9] H.L. Groth, Stress singularities and fracture at interface corners in bonded joints, Inf. J. Adhes. 8 (1988) 107–113.
[10] J.C.W. van Vroonhoven, Stress singularities in bi-material wedges with adhesion and delamination, Fatigue Fracture Engng Mater. Struct. 15 (1992) 159–171.
[11] K. Mizuno, K. Miyazawa, T. Suga, Characterization of thermal stress in ceramic/metal-joint, Journal of the Faculty of Engineering, The University of Tokyo (b) 39–4 (1988) 401–412.
[12] S. Ioka, S. Kubo, K. Ohji, J. Kishimoto, Thermal residual stresses in bonded dissimilar materials and their singularity, JSME Int Journal, Series A 39 (2) (1996) 197–203.
[13] D. Munz, T. Fett, Y.Y. Yang, The regular stress term in bonded dissimilar materials after a change in temperature, Eng. Fract. Mech. 44 (2) (1993) 185–194.
[14] D. Munz, Y.Y. Yang, Stress singularities at the interface in bonded dissimilar materials under mechanical and thermal loading, J. Appl. Mech. 59 (1992) 857–861.
[15] D. Munz, Y.Y. Yang, Stresses near the edge of bonded dissimilar materials described by two stress intensity factors, Inf. J. Fracture 60 (1993) 169–177.
[16] Y.Y. Yang, D. Munz, Determination of the regular stress term in a dissimilar materials joint under thermal loading by the Mellin transformation, J. Therm. Stresses 17 (1994) 321–336.
[17] Y.Y. Yang, D. Munz, The stress distribution in a dissimilar materials joint for complex singular eigenvalues under thermal loading, J. Therm. Stresses 18 (1995) 407–419.
[18] Y.Y. Yang, D. Munz, Stress singularities in a dissimilar materials joint with edge tractions under mechanical and thermal loadings, Int. J. Solids Structures 34 (10) (1997) 1199–1216.
[19] O.T. Iancu, T. Fett, D. Munz, A fracture mechanical treatment of free edge stress singularities applied to a brazed ceramic/metal compound, Int. J. Fract. 46 (1990) 159–172.
[20] D.H. Chen, H. Nisitani, Singular stress field in jointed materials due to thermal residual stress, Transactions of the Japan Society of Mechanical Engineers, Series A 59 (564) (1993) 1937–1941, in Japanese.
[21] D.H. Chen, K. Nonomura, K. Ushijima, Stress intensity factor at the edge point of a bonded strip under thermal loading, JSME International Journal, Series A 44 (4) (2001) 550–555.
[22] Z. Qian, A.R. Akisanya, Analysis of free-edge stress and displacement fields in scarf joints subjected to a uniform change in temperature, Fatigue Fract. Eng. Mater. Struct. 21 (1998) 687–703.
[23] Z. Qian, A.R. Akisanya, An experimental investigation of failure initiation in bonded joints, Acta Mater. 46 (14) (1998) 4895–4904.
[24] E.D. Reedy Jr, Intensity of the stress singularity at the interface corner between a bonded elastic and rigid layer, Eng. Frac. Mech. 36 (4) (1990) 575–583.
[25] K. Oda, T. Shinmoto, N.-A. Noda, Thermal stress intensity factor of an edge interface crack under arbitrary material combination considering double singular stress fields before and after cracking, Acta Mechanica 234 (7) (2023) 3037–3059, https://doi.org/10.1007/s00707-023-03531-4.
[26] Y. Zhang, N.-A. Noda, K. Takaishi, X. Lan, Effect of adhesive thickness on the intensity of singular stress at the adhesive dissimilar joint, Journal of Solid Mechanics and Material Engineering, Vol.4 No.10 (2010), 1467–1479. [Zhang Y., Noda, N.-A., Wu P., Duan M.: Corrigendum to “A mesh-independent technique to evaluate stress singularities in adhesive joints. Int. J. Adhes. 60, 130 (2015)].
[27] N.-A. Noda, F. Ren, R. Takaki, Z. Wang, K. Oda, T. Miyazaki, Y. Sano, Intensity of singular stress field over the entire bond line thickness range useful for evaluating the adhesive strength for plate and cylinder butt joints, Int. J. Adhes. Adhes. 85 (2018) 234–250.
[28] N.-A. Noda, X. Lan, Stress intensity factors for an edge interface crack in a bonded semi-infinite plate for arbitrary material combination, Int. J. Solids Struct. 49 (2012) 1241–1251.
[29] K. Oda, Y. Takahata, Y. Kasamura, N.-A. Noda, Stress intensity factor solution for edge interface crack based on the crack tip stress without the crack, Eng. Fract. Mech. 219 (2019) 106612, https://doi.org/10.1016/j.engfracmech.2019.106612.
[30] T. Yamazaki, Edge singular stress field in jointed materials due to thermal residual stress, Trans. Japan Soc. Mech. Eng. 57 (544 A) (1991) 3029–3036, in Japanese.
[31] J. Dundurs, Discussion of edge-bonded dissimilar orthotropic elastic wedges under normal and shear loading, J Appl Mech. 36 (6) (1969) 650–652, https://doi.org/10.1115/1.3564739.
[32] Y. Suzuki, Adhesive tensile strengths of scarf and butt joints of steel plates (relation between adhesive layer thicknesses and adhesive strengths of joints), JSME Int. J. 30 (265) (1987) 1042–1051.
[33] E.D. Reedy Jr, T.R. Guess, Comparison of butt tensile strength data with interface corner stress intensity factor prediction, International Journal of Solid and Structures 30 (21) (1993) 2929–2936.
[34] E.D. Reedy Jr, T.R. Guess, Interface corner failure analysis of joint strength: Effect of adherend stiffness, Int. J. Fract. 88 (1997) 305–314.
[35] E.D. Reedy Jr, Connection between interface corner and interfacial fracture analyses of an adhesively-bonded butt joint, Int J Solids Struct 37 (17) (2000) 2429–2442, https://doi.org/10.1016/S0020-7683(99)00002-5.
[36] A. Mintzas, D. Nowell, Validation of an Hcr-based fracture initiation criterion for adhesively bonded joints, Eng. Fract. Mech. 80 (2012) 13–27.
[37] N.-A. Noda, T. Miyazaki, R. Li, T. Uchikoba, Y. Sano, Y. Takase, Debonding strength evaluation in terms of the intensity of singular stress at the interface corner with and without fictitious crack, Int. J. Adhes. Adhes. 61 (2015) 46–64.
[38] K. Oda, K. Kamisugi, N.-A. Noda, Analysis of stress intensity factor for interface cracks based on proportional method, Transactions of the Japan Society of Mechanical Engineers, Series A 75 (752) (2009) 476–482, in Japanese.
[39] E.J. Brown, F. Erdogan, Thermal stresses in bonded materials containing cuts on the interface, Int. J. Eng. Sci. 6 (9) (1968) 517–529.